

TABLE 1. Census of CFHT HRCam Images

Field	Filter	Exposures	Airmass	FWHM
Central Field	<i>V</i>	4 × 600 sec	1.19 – 1.35	0".72
Central Field	<i>R</i>	26 × 500 sec	1.08 – 1.31	0".73
Central Field	<i>I</i>	4 × 500 sec	1.35 – 1.48	0".73
East (Background)	<i>R</i>	12 × 600 sec	1.01 – 1.35	0".58

M87 Central Field ( $R < 23.2$ )

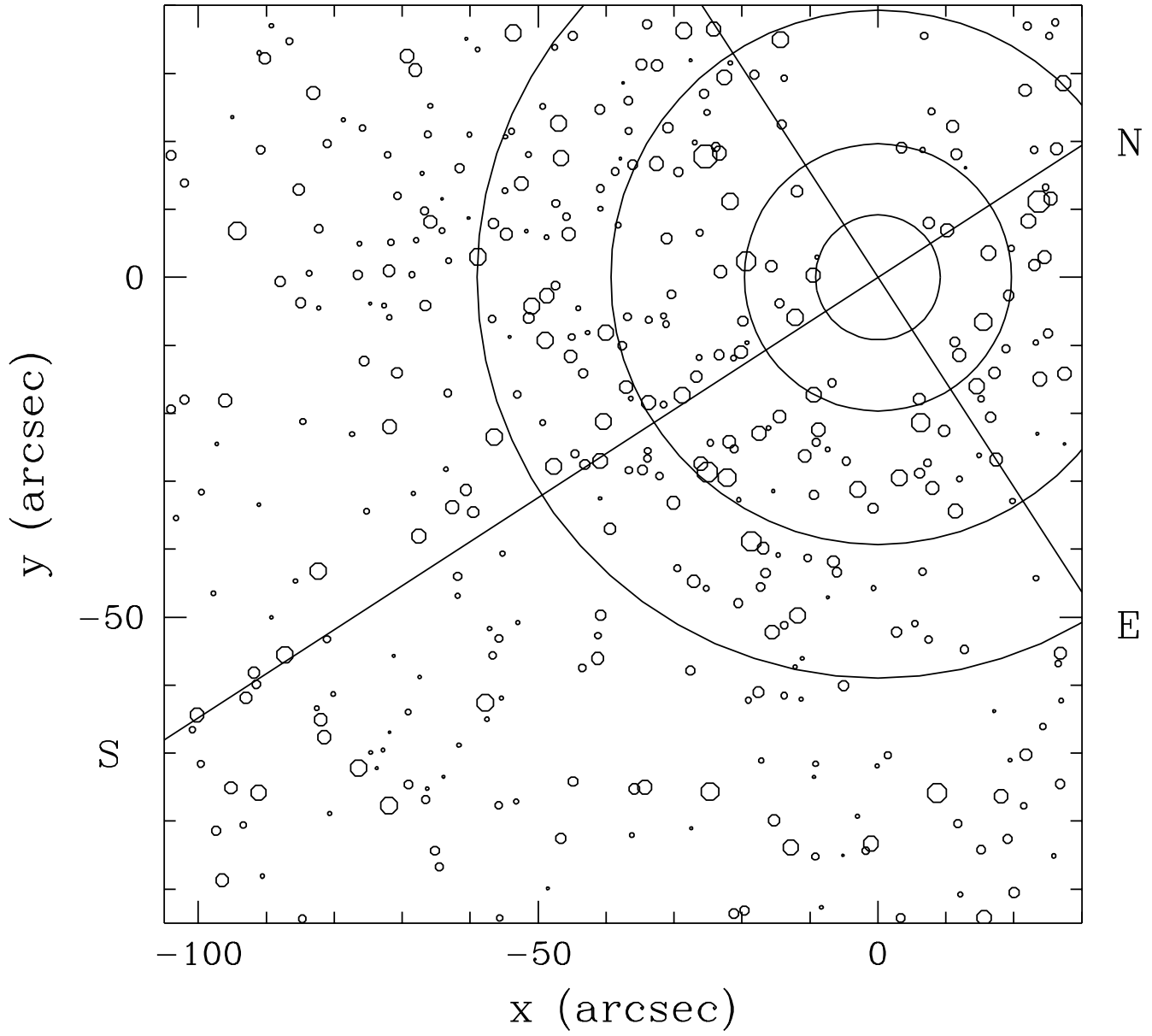


TABLE 2. Photometry of Brightest Clusters

$X''$	$Y''$	$R$	$V - R$	$R - I$	$X''$	$Y''$	$R$	$V - R$	$R - I$
-28.57	-11.67	19.03	0.55	0.74	-36.81	-3.01	20.70	0.47	0.72
3.70	25.88	19.30	0.48	0.70	6.03	15.56	20.73	0.49	0.66
10.59	-36.66	19.60	0.60	0.65	5.28	23.06	20.73	0.47	0.75
22.65	-36.81	19.70	0.62	0.66	87.72	-38.18	20.74	0.63	0.60
-12.34	-15.05	19.83	0.50	0.63	-24.04	-42.40	20.75	0.48	0.71
68.59	-34.00	19.84	0.55	0.65	-58.04	-19.33	20.76	–	–
21.54	-6.39	19.95	0.46	0.58	-43.58	-0.46	20.77	0.50	0.77
12.84	-34.67	20.04	0.54	0.58	-5.28	-7.87	20.77	–	–
50.22	-61.90	20.09	0.55	0.47	9.93	-27.16	20.79	0.52	0.86
-56.79	-75.42	20.13	0.71	0.65	35.23	-9.19	20.80	0.41	0.80
14.15	9.40	20.18	0.42	0.78	44.48	-69.60	20.80	0.52	0.47
26.25	-102.68	20.26	0.50	0.46	25.69	11.83	20.81	0.46	0.71
21.28	-82.58	20.27	0.45	0.47	-31.55	-18.29	20.81	0.54	0.79
-0.69	-103.44	20.29	0.49	0.56	-2.73	-38.39	20.81	–	0.63
-34.35	-47.79	20.29	0.47	0.60	-4.62	-77.45	20.83	0.53	0.66
-10.82	-60.20	20.33	0.51	0.55	-27.84	-9.68	20.83	0.62	0.61
-1.47	-13.44	20.35	0.36	0.81	74.10	-26.36	20.84	0.57	0.75
-45.77	-4.28	20.36	0.61	0.73	-20.46	-72.29	20.85	0.46	0.62
19.17	-103.42	20.37	0.49	0.52	-64.80	-40.48	20.85	0.40	0.65
-8.35	-92.65	20.38	0.52	0.49	35.53	-41.50	20.86	0.51	0.62
-21.02	-12.21	20.39	0.49	0.67	-0.27	-119.11	20.88	0.47	0.64
-59.17	-25.51	20.39	0.97	1.30	14.28	-19.57	20.91	0.45	0.77
-18.68	-46.16	20.41	0.51	0.64	8.97	-36.83	20.92	0.52	0.74
-0.90	-33.62	20.44	0.47	0.51	26.99	15.26	20.92	0.58	0.67
-23.97	-45.10	20.44	0.56	0.60	-39.97	-36.56	20.92	0.47	0.59
-4.00	-45.45	20.46	0.58	0.71	4.28	27.58	20.93	0.45	0.70
-2.40	-55.19	20.48	0.59	0.69	-67.76	-55.01	20.94	0.45	0.53
-44.39	-27.15	20.49	0.55	0.64	12.64	-105.18	20.95	0.39	0.48
35.53	-37.00	20.50	0.53	0.73	-0.10	12.27	20.97	1.09	0.15
24.77	-19.50	20.50	0.50	0.58	-29.90	-34.75	20.97	0.50	0.51
21.55	3.43	20.51	0.51	0.62	-36.85	-90.51	20.99	0.58	0.74
-39.90	-29.61	20.53	0.49	0.50	-5.51	-70.95	21.02	0.60	0.62
26.65	-13.44	20.53	0.39	0.60	-7.68	6.38	21.03	–	–
-14.75	-38.10	20.56	0.50	0.46	-42.48	-50.86	21.03	0.58	0.69
63.59	-56.38	20.56	0.44	0.44	-62.44	-40.58	21.06	0.51	0.50
14.25	-117.76	20.57	0.50	0.57	8.60	-31.55	21.06	0.97	0.37
-8.98	38.34	20.58	0.59	0.72	32.13	-0.02	21.06	0.36	0.54
9.55	-17.35	20.59	0.44	0.50	11.65	-43.31	21.06	0.47	0.50
69.52	-46.20	20.61	0.48	0.52	-1.56	-22.94	21.06	0.57	0.87
0.63	-49.05	20.67	0.53	0.73	30.55	-10.16	21.06	0.36	0.69

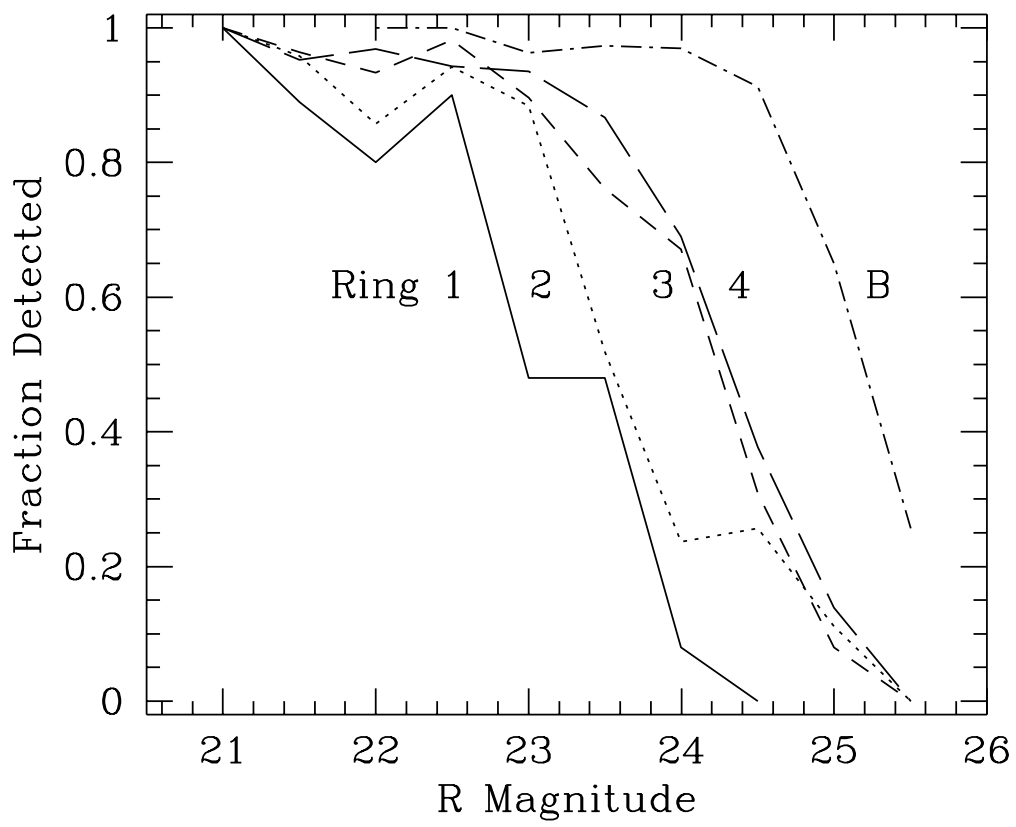


TABLE 3. Definition of Radial Zones

Zone	$r$ (px)	$r$ (arcsec)	$A$ (arcmin <sup>2</sup> )	$\alpha$	$m_0$
Ring 1	70 – 150	9.17 – 19.65	0.242	1.812	23.11
Ring 2	150 – 300	19.65 – 39.30	0.822	1.465	23.62
Ring 3	300 – 450	39.30 – 58.95	0.856	1.590	24.16
Ring 4	450 – 1080	58.95 – 141.5	2.855	1.460	24.28
Bkgd	–	–	4.96	1.975	25.19

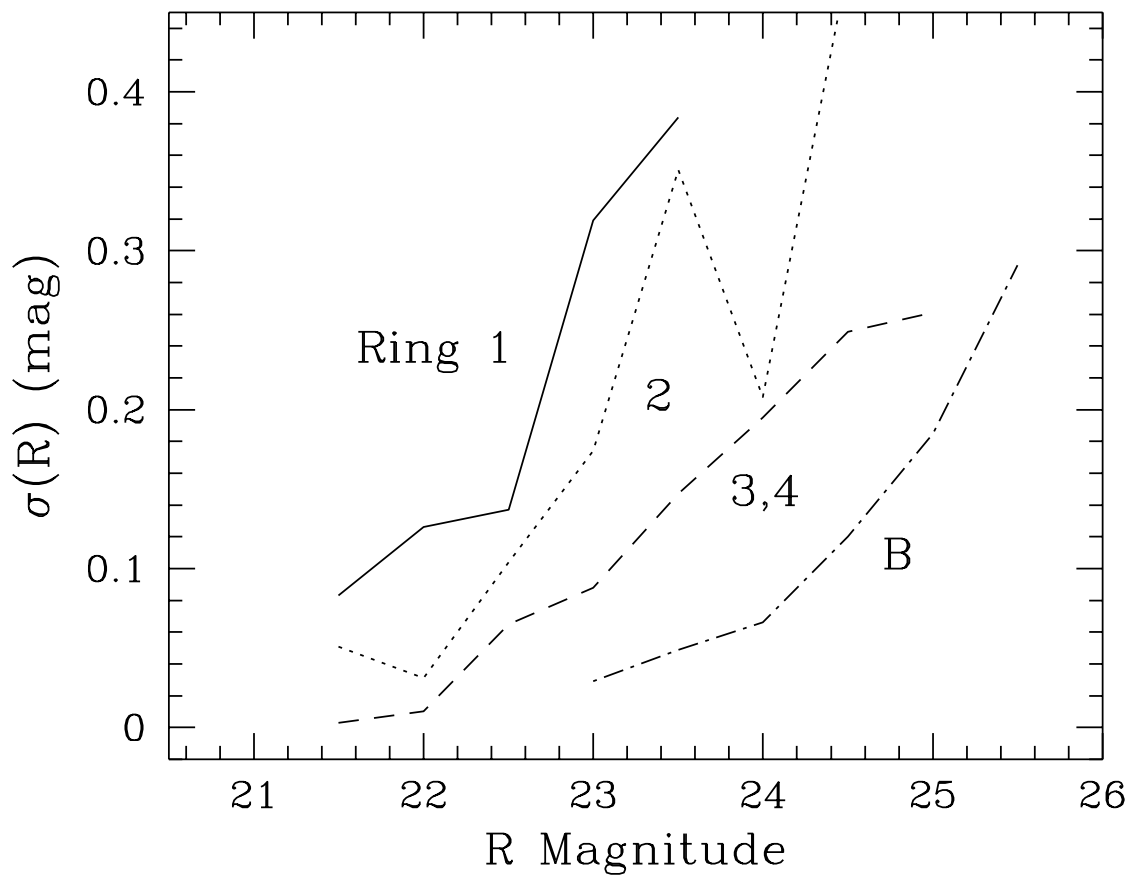


TABLE 4. The M87 GCLF as a Function of Radius

$R$	Ring 1	Ring 2	Ring 3	Ring 4	Bkgd
19.2	$0.0 \pm 1.7$	$2.0 \pm 1.7$	$0.0 \pm 1.7$	$0.0 \pm 2.0$	$0.0 \pm 1.0$
19.6	$0.0 \pm 1.7$	$1.0 \pm 1.7$	$1.0 \pm 1.7$	$0.0 \pm 2.0$	$0.0 \pm 1.0$
20.0	$2.0 \pm 1.7$	$2.0 \pm 1.7$	$0.0 \pm 1.7$	$2.0 \pm 2.0$	$0.0 \pm 1.0$
20.4	$1.0 \pm 1.7$	$6.1 \pm 3.0$	$11.1 \pm 4.0$	$9.1 \pm 3.8$	$0.0 \pm 1.0$
20.8	$2.9 \pm 2.1$	$11.7 \pm 4.2$	$5.5 \pm 3.0$	$10.4 \pm 4.4$	$3.0 \pm 1.7$
21.2	$7.1 \pm 3.2$	$14.1 \pm 4.6$	$8.9 \pm 3.7$	$13.6 \pm 4.7$	$1.0 \pm 1.0$
21.6	$4.1 \pm 2.5$	$11.3 \pm 4.1$	$11.2 \pm 4.1$	$22.4 \pm 5.8$	$0.0 \pm 1.0$
22.0	$5.1 \pm 2.8$	$15.1 \pm 4.9$	$24.0 \pm 6.0$	$27.9 \pm 6.7$	$3.0 \pm 1.7$
22.4	$8.9 \pm 3.8$	$33.8 \pm 7.3$	$19.2 \pm 5.4$	$31.8 \pm 7.1$	$2.0 \pm 1.4$
22.8	$15.0 \pm 5.5$	$29.1 \pm 6.9$	$18.5 \pm 5.3$	$63.9 \pm 10.0$	$2.0 \pm 1.4$
23.2	$22.2 \pm 9.9$	$35.8 \pm 8.4$	$25.0 \pm 6.4$	$44.1 \pm 8.8$	$6.1 \pm 2.5$
23.6	—	$29.0 \pm 10.6$	$21.0 \pm 6.4$	$43.9 \pm 9.5$	$11.3 \pm 3.4$
24.0	—	—	$17.1 \pm 7.7$	$32.8 \pm 10.0$	$18.8 \pm 4.4$
24.4	—	—	—	$21.5 \pm 15.4$	$48.9 \pm 7.3$
Total	$68.4 \pm 13.5$	$191.1 \pm 19.5$	$162.5 \pm 17.3$	$323.3 \pm 28.3$	$96.1 \pm 10.3$
Rel.Area	0.049	0.166	0.173	0.576	1.000

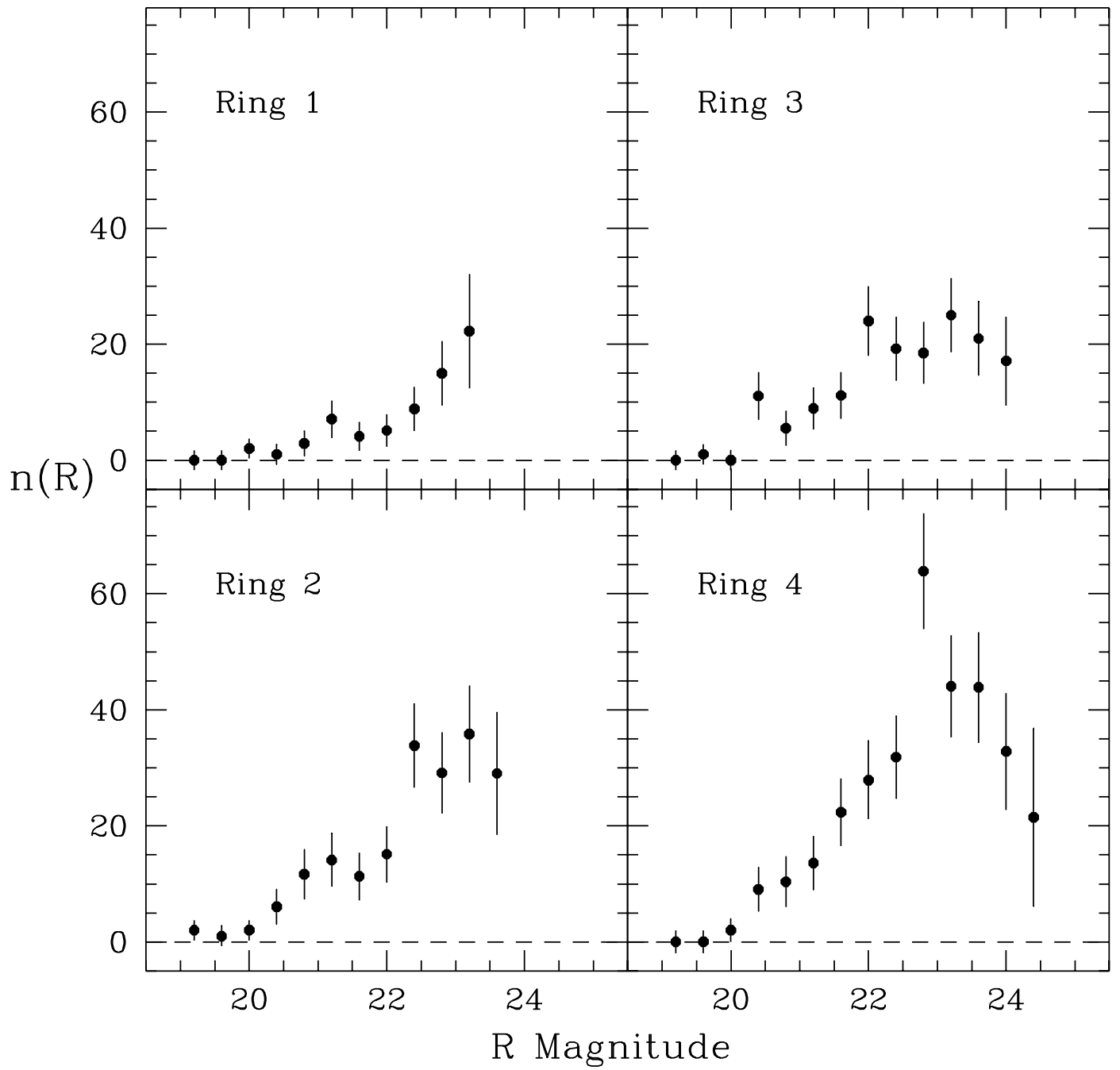


TABLE 5. Cluster Metallicity Versus Radius

$r''$	N	$\langle V - I \rangle$	$\sigma(V - I)$	$[\text{Fe}/\text{H}]_{V-I}$	$\sigma[\text{Fe}/\text{H}]$
20.5	14	$1.139 \pm 0.031$	0.122	$-0.34 \pm 0.18$	0.66
28.4	17	$1.164 \pm 0.036$	0.146	$-0.20 \pm 0.19$	0.79
38.1	18	$1.145 \pm 0.027$	0.155	$-0.31 \pm 0.20$	0.85
47.3	22	$1.139 \pm 0.038$	0.168	$-0.34 \pm 0.19$	0.91
60.0	21	$1.148 \pm 0.015$	0.163	$-0.29 \pm 0.20$	0.90
78.5	19	$1.045 \pm 0.022$	0.148	$-0.86 \pm 0.19$	0.81
99.5	22	$1.089 \pm 0.032$	0.181	$-0.62 \pm 0.21$	0.99

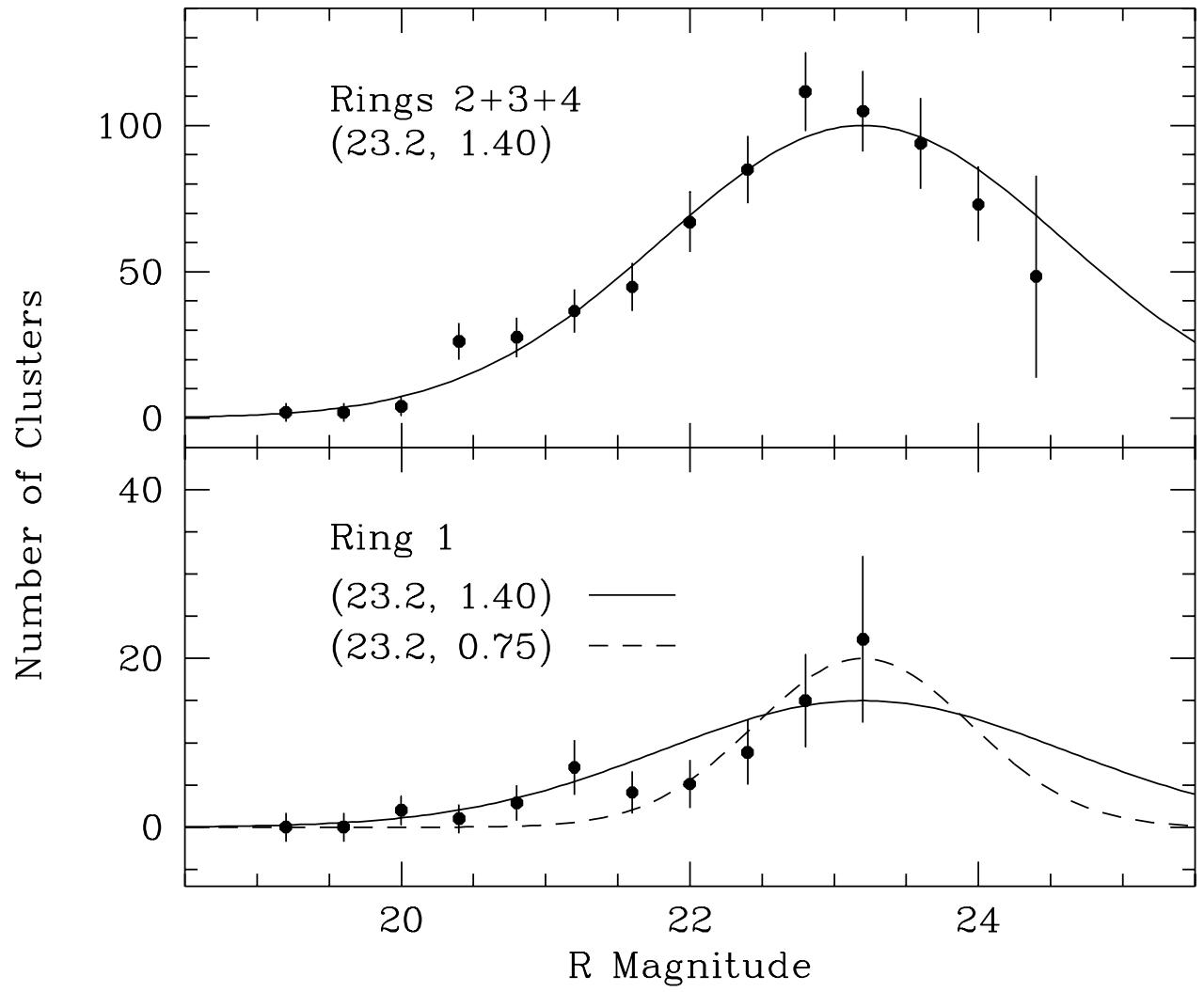
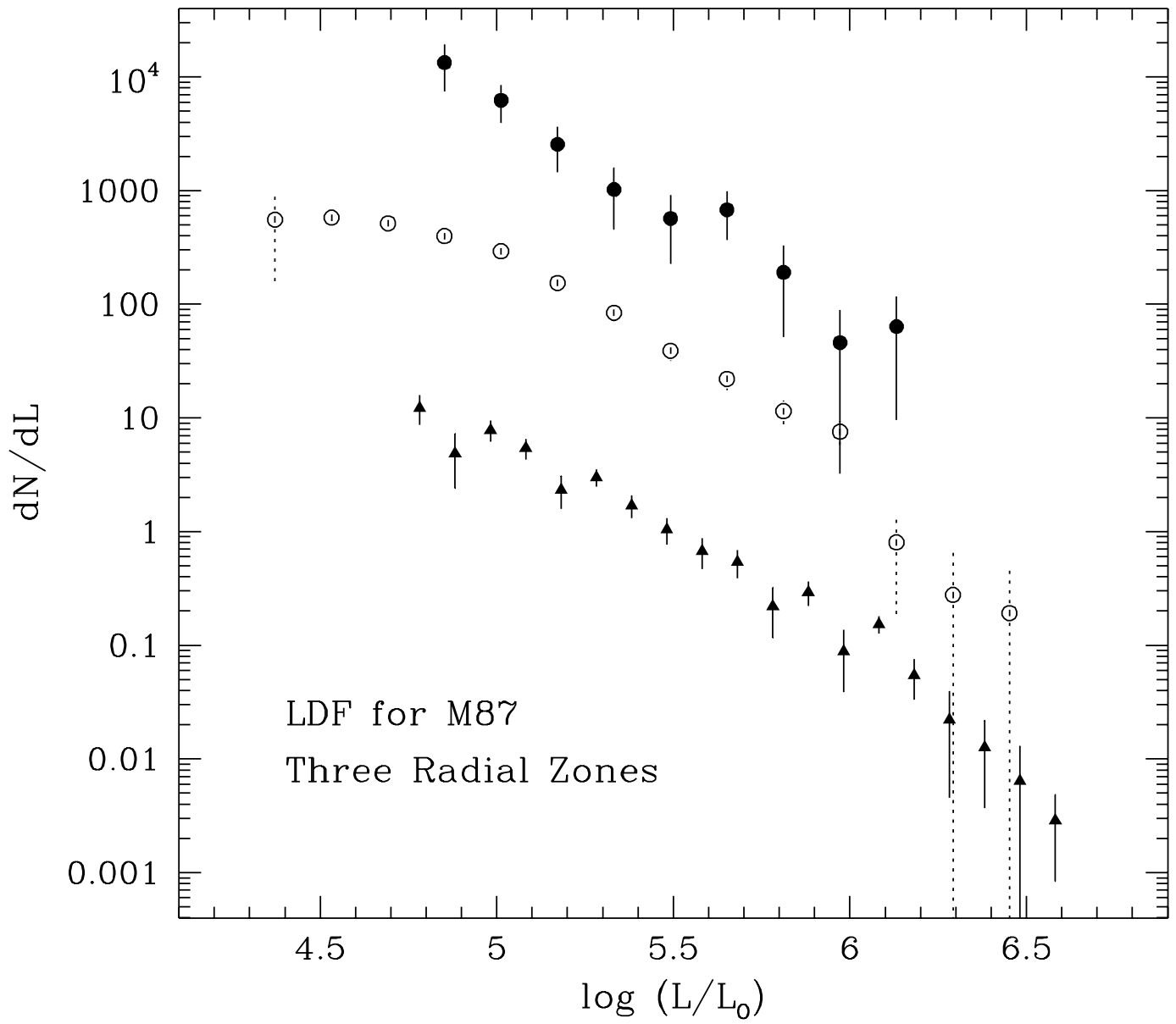


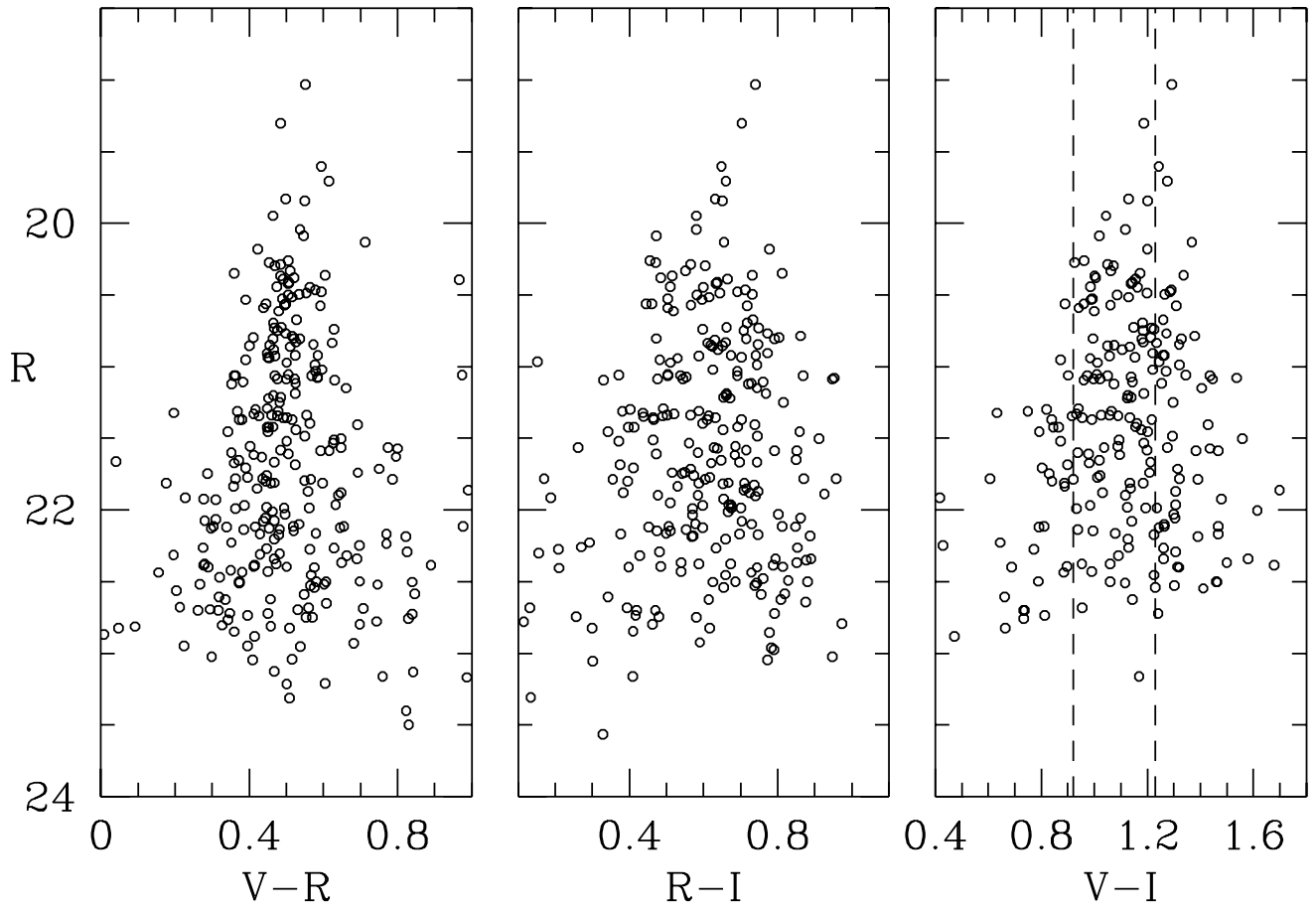
TABLE 6. Globular Cluster Data for Selected BCGs

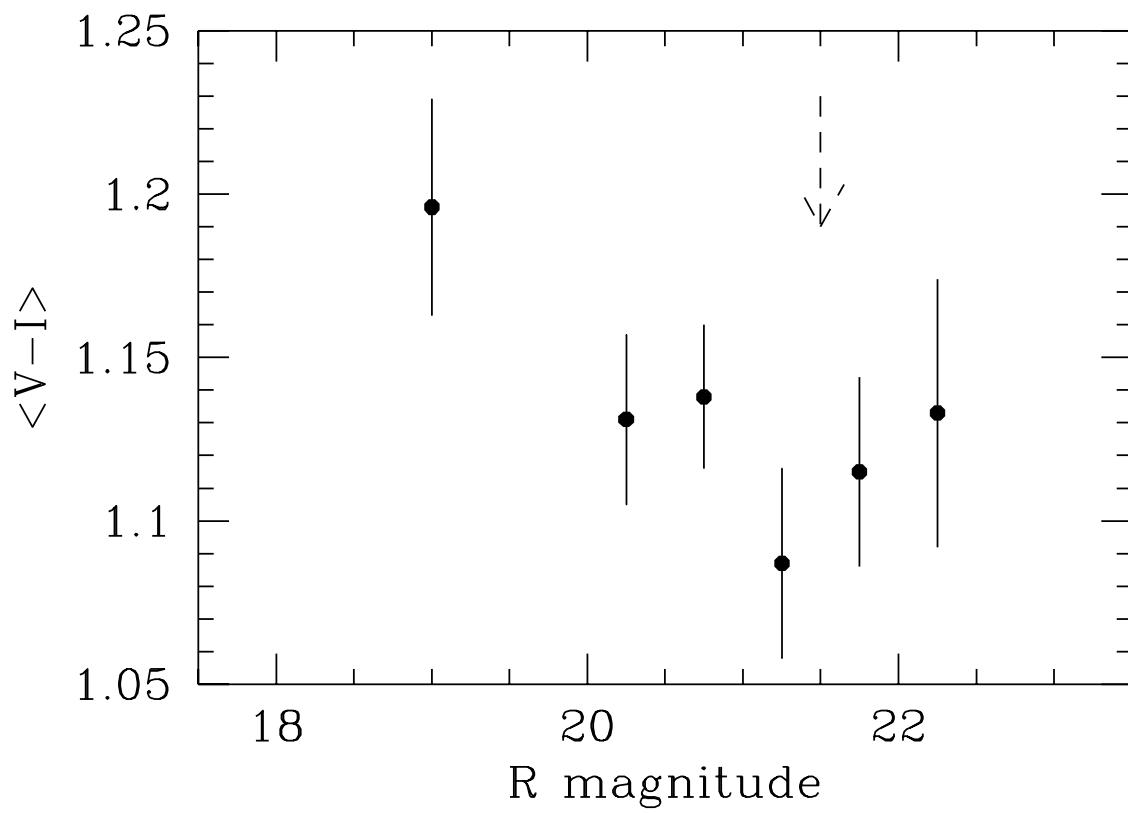
Galaxy	Cluster	$M_V^T$	$S_N$	$S_N^{40}$	$\sigma_{cl}$ (km s $^{-1}$ )	ICM $kT$ (keV)
N0524	CfA13	-22.1	$6.4 \pm 1.4$	$4.9 \pm 1.1$	$206 \pm 110$ (1)	6.7 (6)
N1275	A426 (Perseus)	-23.1	$4.3 \pm 1.4$	$3.3 \pm 1.1$	$1026 \pm 80$ (2)	6.7 (6)
N1399	S373 (Fornax)	-21.7	$11.1 \pm 2.1$	$10.6 \pm 1.9$	$310 \pm 30$ (2)	1.1 (6)
N1407	Eridanus	-22.1	$4.0 \pm 1.3$	$3.1 \pm 1.0$	$264 \pm 30$ (2)	0.9 (7)
N3311	A1060 (Hydra)	-22.4	$15.0 \pm 6.0$	$11.5 \pm 4.6$	$610 \pm 50$ (2)	3.9 (6)
N3379	CfA68 (Leo)	-20.7	$1.3 \pm 0.7$	$1.0 \pm 0.5$	$120 \pm 70$ (1,3)	–
N4073	MKW4	-23.1	$4 \pm 2$ :	$3.1 \pm 1.5$ :	$525 \pm 60$ (2)	1.7 (6)
N4486	Virgo	-22.4	$14.1 \pm 1.6$	$9.1 \pm 1.3$	$632 \pm 40$ (2)	3.0 (6)
N5128	Centaurus	-22.0	$2.6 \pm 0.6$	$2.0 \pm 0.5$	$90 \pm 32$ (4)	–
U9799	A2052	-23.4	$20.7 \pm 6.5$	$15.9 \pm 5.0$	$750 \pm 180$ (5)	3.1 (6)
U9958	A2107	-23.4	$12.2 \pm 5.6$	$9.4 \pm 4.3$	$622 \pm 70$ (2)	4.2 (6)

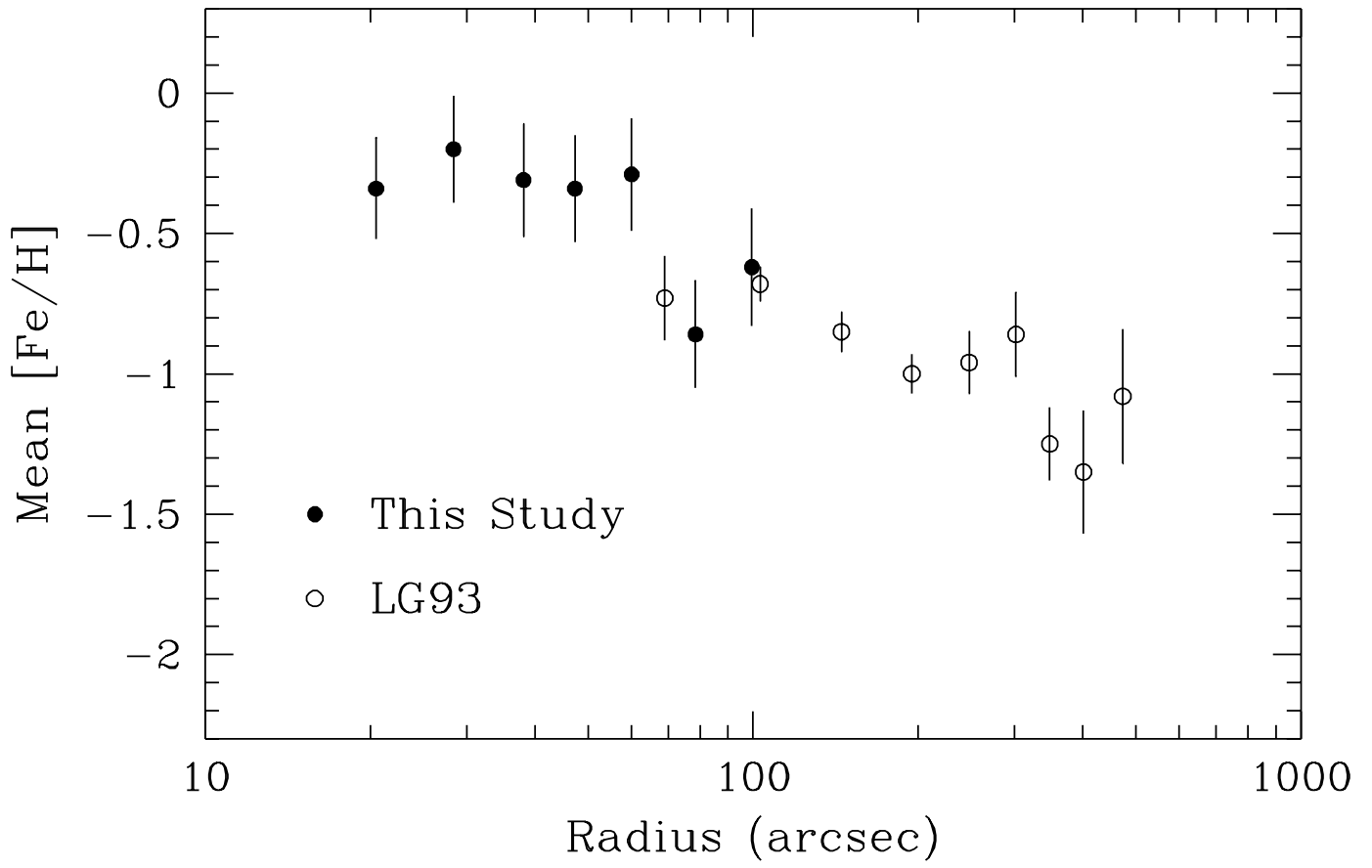
References for Table 6.

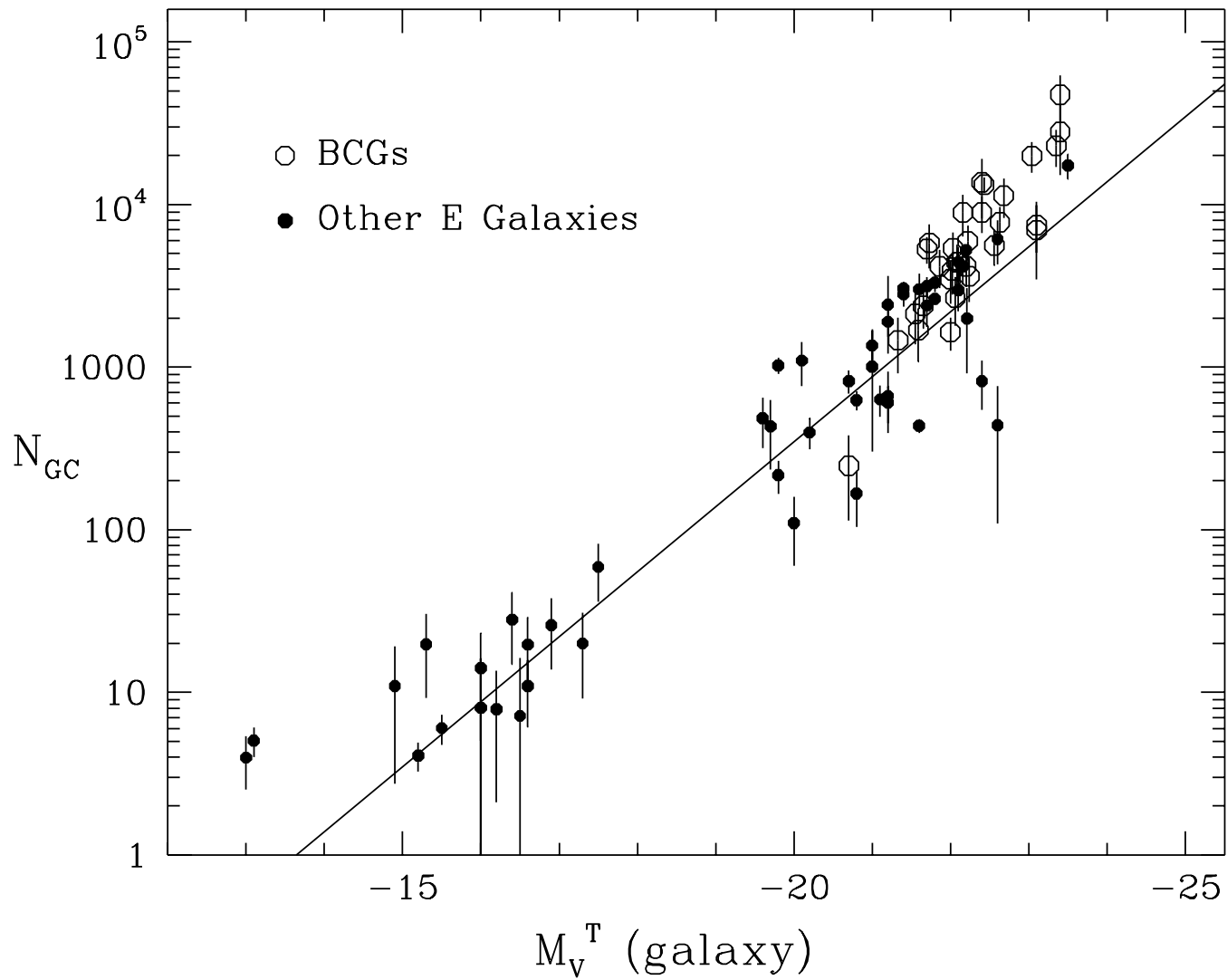
(1) Geller & Huchra 1983; (2) Fadda *et al.* 1996; (3) de Vaucouleurs 1975; (4) Hesser *et al.* 1984; (5) Girardi *et al.* 1993; (6) Harris *et al.* 1995; (7) Davis & White 1996

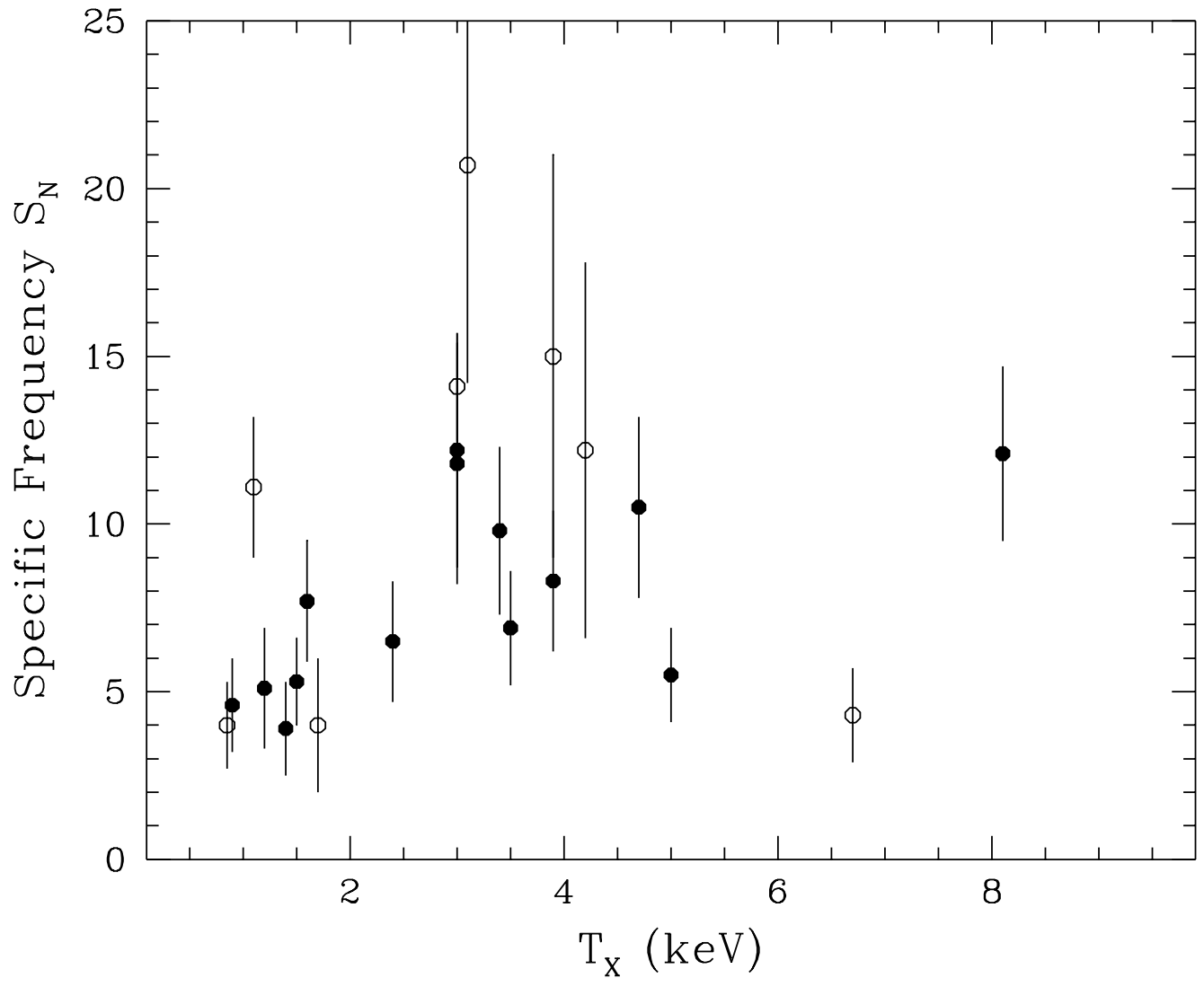


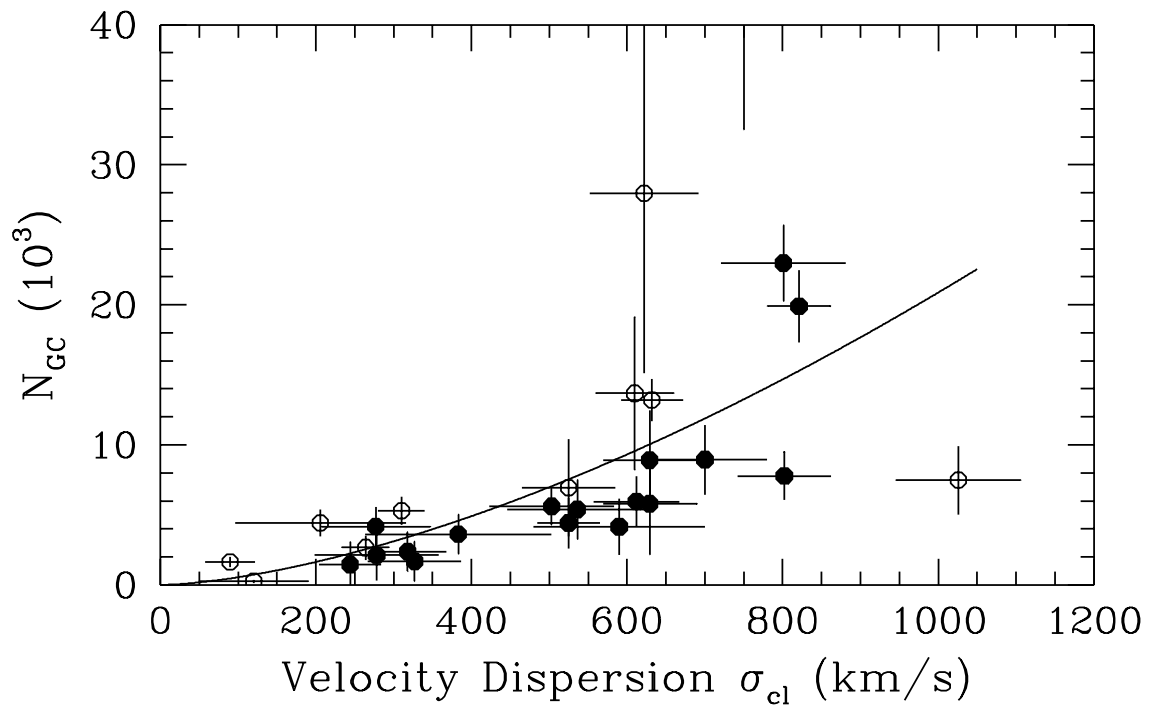
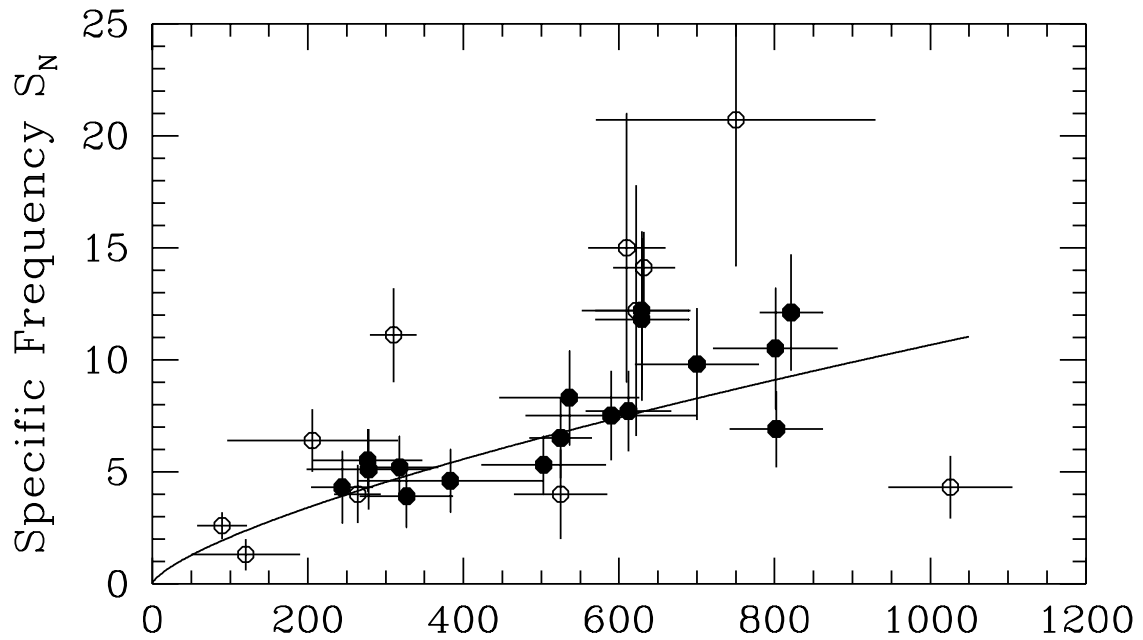


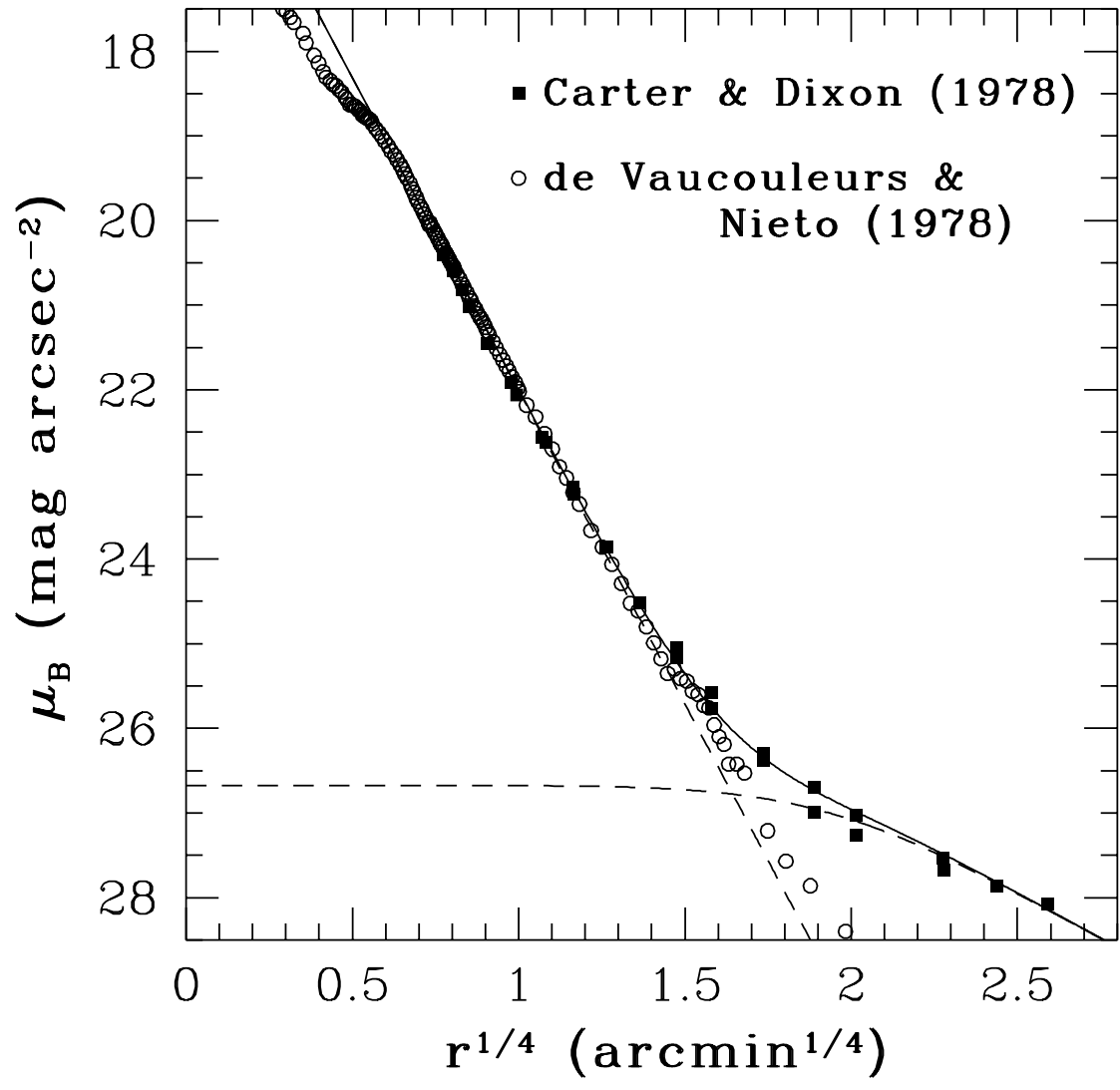


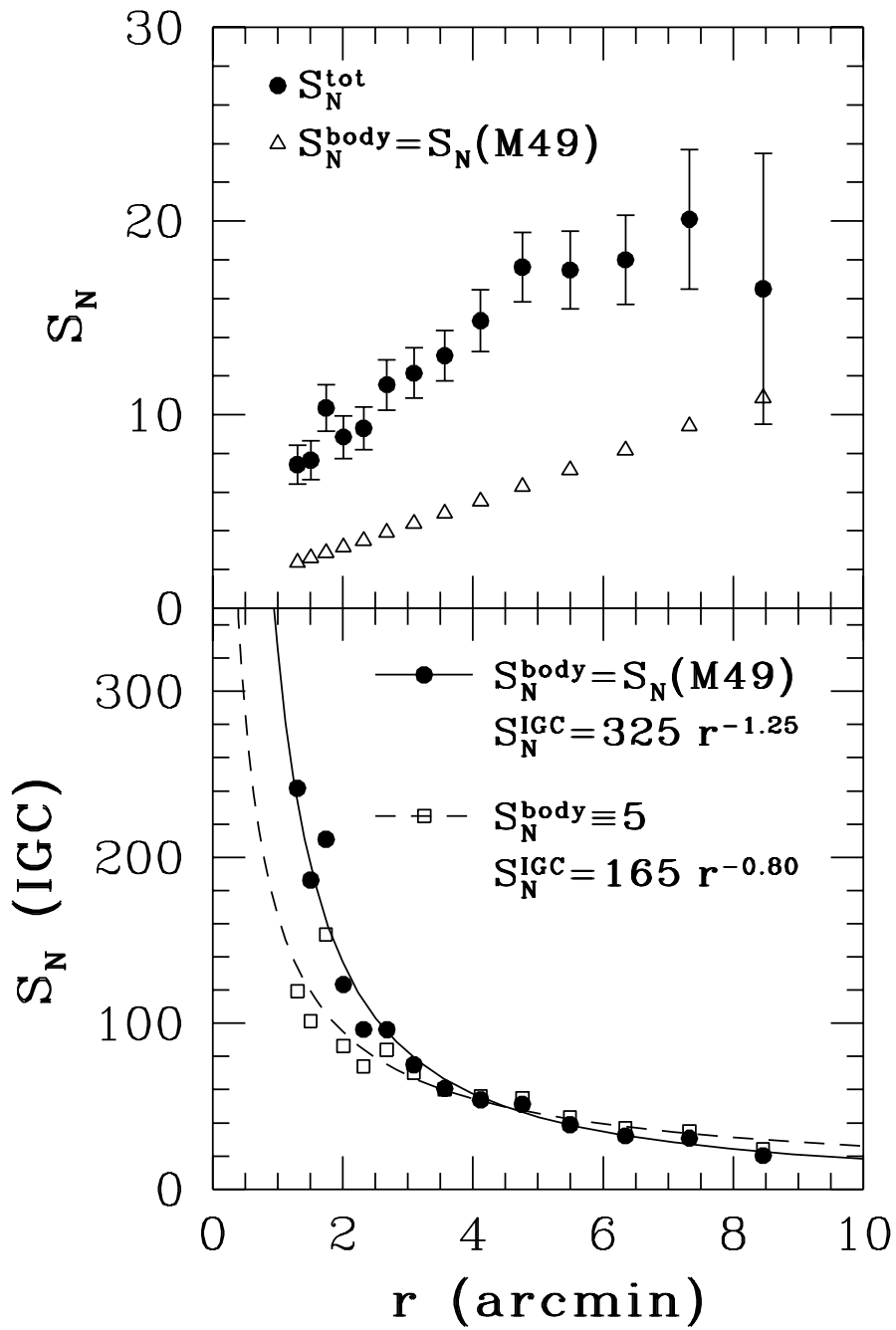


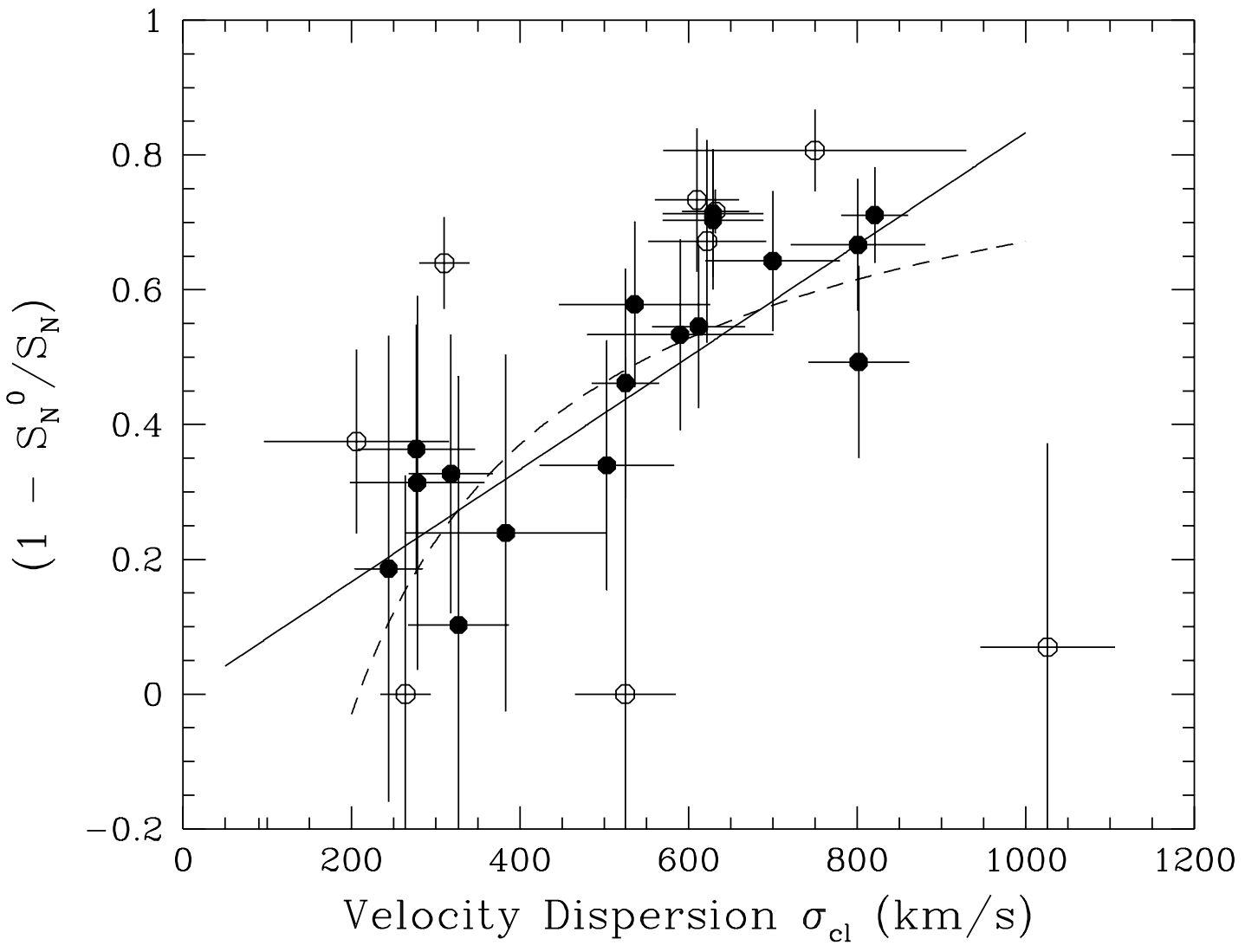


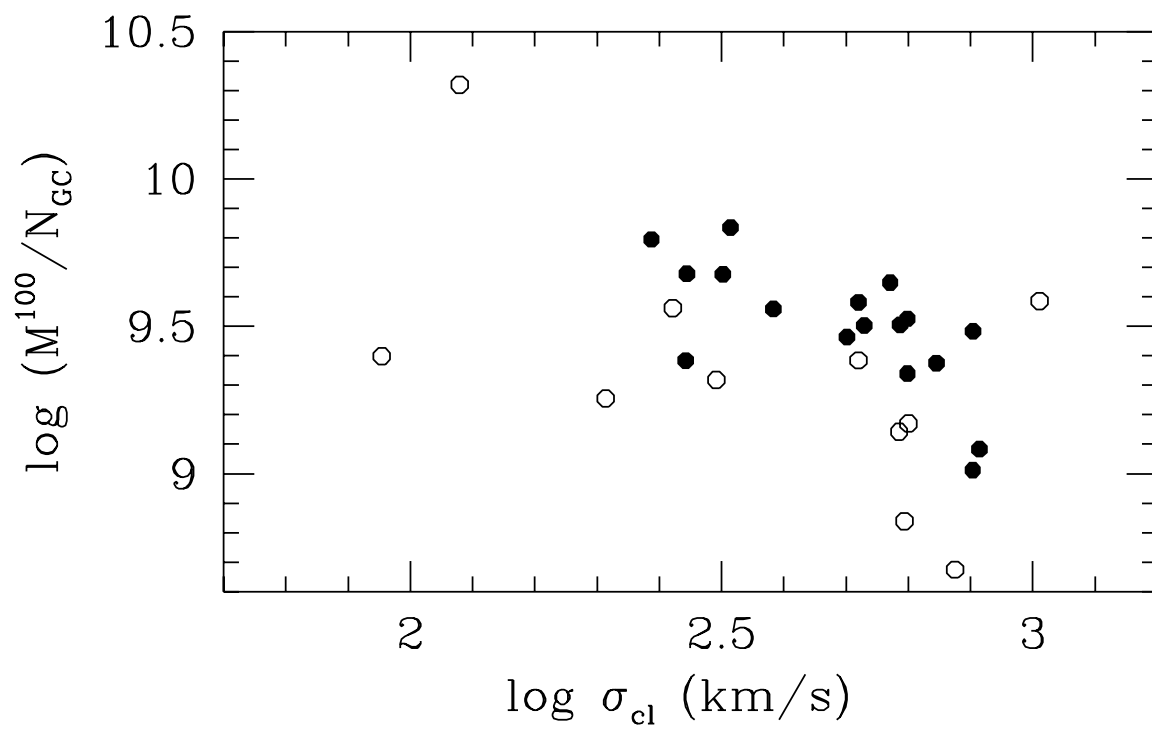
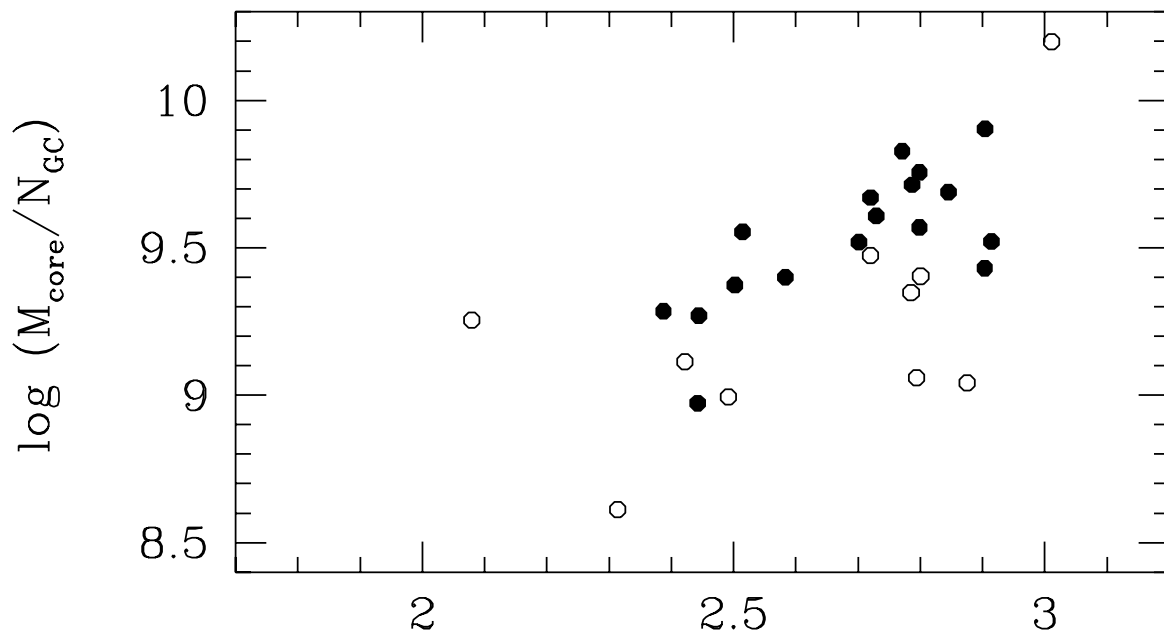












# M87, Globular Clusters, and Galactic Winds: Issues in Giant Galaxy Formation

William E. Harris<sup>1</sup>

Department of Physics & Astronomy, McMaster University, Hamilton, Ontario L8S 4M1  
Electronic mail: harris@physics.mcmaster.ca

Gretchen L. H. Harris<sup>1</sup>

Department of Physics, University of Waterloo, Waterloo, Ontario N2L 3G1  
Electronic mail: glharris@astro.uwaterloo.ca

Dean E. McLaughlin<sup>1,2</sup>

Department of Physics & Astronomy, McMaster University, Hamilton, Ontario L8S 4M1  
Electronic mail: dean@crabneb.berkeley.edu

arXiv:astro-ph/9801214v1 22 Jan 1998

---

<sup>1</sup>Visiting Astronomer, Canada-France-Hawaii Telescope, operated by the National Research Council of Canada, le Centre National de la Recherche Scientifique de France, and the University of Hawaii.

<sup>2</sup>Hubble Fellow; now at Department of Astronomy, University of California, Berkeley CA 94720

## ABSTRACT

We have used the High Resolution Camera at the Canada-France-Hawaii Telescope to obtain  $VRI$  photometry of the globular clusters in the innermost  $140''$  of the M87 halo. The results are used to discuss several issues concerning the formation and evolution of globular cluster systems in supergiant ellipticals like M87. Our principal results are as follows: (1) From our deep  $R$ -band photometry of the cluster population, we find *no significant change* in the globular cluster luminosity function (GCLF) with galactocentric radius, for cluster masses  $M \gtrsim 10^5 M_\odot$ . This result places constraints on current theoretical predictions of the rate of cluster evolution by tidal shocking and evaporation, indicating that the main effects of dynamical evolution may be only on lower-mass clusters ( $\lesssim 10^5 M_\odot$ ) that are below the faint limit of most current observations. (2) Combining our  $(V - I)$  color indices with other data in the literature, we derive the metallicity gradient and mean metallicity of the clusters from  $r = 9''$  out to  $r \simeq 500''$  ( $\sim 0.7$  to  $35$  kpc). Within the core radius  $r_c = 1'$  of the globular cluster system, the metallicity distribution is uniform, but at larger radii the mean metallicity declines steadily as  $Z/Z_\odot \sim r^{-0.9}$ . (3) The various options for explaining the existence of high specific frequency galaxies like M87 are evaluated. We argue that alternatives involving secondary evolution (such as the formation of many globular clusters during mergers, or the existence of a population of intergalactic globular clusters centered on the same location as the central elliptical) are capable of modifying the characteristics of the GCS in distinctive ways, but are not likely to be the primary explanation for high- $S_N$  galaxies. (4) We offer a new explanation for the large observed  $S_N$  range among brightest cluster ellipticals (BCGs). It is suggested that these central supergiant E galaxies formed in an exceptionally turbulent or high-density environment which favored a very rapid initial star formation burst. As a result, a much higher than average fraction of the protogalactic gas was driven out in a galactic wind not long after the first globular clusters were formed, thus artificially boosting the specific frequency of the remaining galaxy. From a total sample of 30 BCGs, we derive empirical scaling relations which relate to this hypothesis. Our analysis favors the view that BCGs began forming at redshifts  $z \gtrsim 5$ , distinctly earlier than most other galaxies.

*Subject headings:* Stellar Systems: Globular clusters; Normal galaxies

## 1. INTRODUCTION

Although much is now known about the characteristics of globular cluster systems (GCSs) in large galaxies (e.g., Harris 1991), the properties of globular clusters in the *inner* regions of these galaxies are still poorly understood, for the simple reason that such objects are extremely difficult to observe against the strong background light of their host galaxy. The innermost few kiloparsecs are, however, precisely the regions where the strongest traces of dynamical evolution of the clusters should be seen, and are thus of considerable interest as tests of the many dynamical models now in the literature (see, e.g., Okazaki & Tosa 1995; Capriotti & Hawley 1996; Gnedin & Ostriker 1997; Ostriker & Gnedin 1997; Vesperini 1997 for comprehensive recent discussions). Do the inner clusters exhibit the expected history of disruption through their spatial distribution, luminosity distribution (GCLF), orbital distribution function, or local specific frequency? What fraction of the globular clusters that might have initially formed in these inner regions survived successfully to the present day? At present there are few galaxies for which relevant GCS data exist to constrain the models strongly.

From the theoretical side, an additional major problem is to decide which of the systemic properties of the GCS that we see today (spatial distribution, GCLF, and so on) are due to the formation epoch, and how much to subsequent dynamical evolution. There are now plausible theoretical and observational grounds to suppose that the *formation* mechanism for globular clusters in protogalaxies was largely independent of location in the halo (Harris & Pudritz 1994 [hereafter HP94]; McLaughlin & Pudritz 1996; Elmegreen & Efremov 1997). But as soon as clusters form, they fall prey to a variety of erosion mechanisms, especially tidal shocking, early mass loss driven by high-mass stars, and (in disk galaxies) disk shocking. In the innermost  $\lesssim 2$  kpc, dynamical friction may also play a role in removing the most massive clusters (e.g., Capriotti & Hawley 1996; Capuzzo-Dolcetta & Tesserì 1997). All these mechanisms depend sensitively on galactocentric distance  $R_{gc}$  and the tidal field. Many theoretical discussions (cf. the references cited above) have raised the possibility that the inner-halo structure of the GCS might be completely dominated by dynamical evolution, i.e. that the great majority of the clusters originally present there might now be gone. For M87 particularly, several recent papers discuss the possibility that the entire massive nucleus might have built up from dissolved clusters (see Capuzzo-Dolcetta 1993; McLaughlin 1995; Capuzzo-Dolcetta & Vignola 1997). An analysis specifically tuned to giant ellipticals such as M87 (Murali & Weinberg 1997) also suggests that both the total population and mass spectral index of the GCS should suffer quite significant changes with time because the rates of dynamical erosion depend on galactocentric distance.

On observational grounds, it is now clear that GCSs in large galaxies display spatial

distributions which typically have large *core radii*, typically a few kpc in size (e.g., Lauer & Kormendy 1986; Harris *et al.* 1991; Grillmair *et al.* 1994a; McLaughlin 1995; Forbes *et al.* 1996). It has frequently been suggested that this feature might have resulted from wholesale cluster erosion at small  $R_{gc}$ , a view which has been argued by the dynamicists since the early paper of Tremaine *et al.* (1975). Some recent continue to favor such an interpretation (e.g., Capuzzo-Dolcetta 1993 and Capuzzo-Dolcetta & Tesserì 1997), while other discussions favor considerably more modest effects of destruction (e.g. McLaughlin 1995). Clearly, the possibility that many clusters *might* have been destroyed in these inner regions does not require that a large initial population of clusters *must* have existed in the core regions of these galaxies; the question is still open, and the direct evidence that we are left with today is highly circumstantial at best. An alternate approach (though one which has not yet been explored in the same detail; see HP94) is that a similar result could have arisen from the details of the cluster formation epoch. For example, the strong tidal field could have inhibited the initial buildup of globular-like protoclusters, or early mass loss could have evaporated them rapidly in the first few  $\sim 10^8$  y of their history. Direct observational evidence of cluster formation in the inner regions of the merger remnant NGC 7252 recently presented by Miller *et al.* (1997) is intriguingly consistent with such a view, and deserves much closer evaluation as well as theoretical modelling.

A somewhat more direct piece of evidence that dynamical evolution has dominated the construction of the GCLF that we now observe – in essence, something closer to a “smoking gun” signature of erosive processes – would be a progressive change in the *shape* of the GCLF with galactocentric distance, i.e. the relative numbers of clusters of different mass. If the initial mass distribution of the clusters is at least roughly independent of galactocentric distance (e.g., HP94; Elmegreen & Efremov 1997; McLaughlin & Pudritz 1996; DiFazio 1986; Ostriker & Gnedin 1997), then such a change can only have arisen from dynamical evolution. On the theoretical side, this is the approach taken by several other authors (e.g., Capriotti & Hawley 1996, Vesperini 1997, or Ostriker & Gnedin 1997). We now need better and more extensive data to compare with these simulations.

Within the Milky Way, the population of globular clusters at all  $R_{gc}$  is quite well defined over the full range of luminosities, but is too small a sample to provide strong statistical tests (e.g., Gnedin & Ostriker 1997; Kavelaars & Hanes 1997). M87 itself is perhaps the best available testbed for these ideas, because of its simple gE structure, relatively nearby location, and enormous cluster population: statistically useful numbers of globular clusters can be traced in to within  $\sim 1$  kpc of its center, and the GCLF can be studied to faint levels. In this paper, we present new photometric data for the inner-halo GCS of M87 specifically designed to address these issues.

The paper is cast in two major parts. In Secs. 2–4, we present our new photometric data for M87, the luminosity function of the inner-halo GCS, and the color and metallicity distributions. Then in Sec. 5, we take up the long-standing problem of understanding how M87 and other central-supergiant ellipticals can generate such exceptionally large populations of globular clusters in all parts of their halos (the “specific frequency problem”). After assessing various suggestions in the literature, we conclude that the basic GCS characteristics were most likely built in at birth, and suggest that they may have been influenced strongly by the early galactic wind in such galaxies.

## 2. THE DATA

### 2.1. Observations and Calibration

The observations for this study were obtained at the Canada-France-Hawaii Telescope during 1993 March 28/29 and 29/30. The High Resolution Camera (McClure *et al.* 1989) was used at prime focus, with the red-sensitive SAIC1 CCD detector: this CCD (now decommissioned) had an 18 micron pixel size, a  $1020 \times 1020$  format after bias subtraction and trim, readnoise rms  $5.5e^-$ , and gain  $1.9 e^-$  per adu. With a scale of  $0''.131$  per pixel in HRCam, the total field size was  $2'.23$  on a side, corresponding to  $9.7 \times (D/15)$  kpc if M87 is at a distance of  $D$  Mpc. This size was comfortably enough to enclose the entire central region of the M87 GCS, which has a core radius  $r_c \simeq 1'$  (McLaughlin 1995).

For our deep GCLF observations, we used the  $R$ -band, which was the standard filter nearest the peak sensitivity of the SAIC1 CCD. The GCLF turnover (peak frequency of cluster numbers per unit magnitude) is at  $V \simeq 23.7$  (Whitmore *et al.* 1995), or  $R \simeq 23.2$  for  $(V - R) \simeq 0.5$  (see below). To reach well past this limit while avoiding saturation from the bright background light of M87, we used a long string of relatively short exposures ( $26 \times 500$  seconds) with individual frames shifted along a sequence of 7 different positions separated by several arcseconds. The individual exposures were then re-registered and median-combined to construct a final deep image. This image, which we will refer to as the “central field,” is shown in Fig. 1 with the smooth galaxy light subtracted. The field center is actually almost  $1'$  due south of the M87 nucleus, a choice which was governed by the location of the best available nearby guide star to drive the HRCam tip-tilt correction during the exposures.

Although the population of detected starlike images in the M87 central field is totally dominated by globular clusters, an accurate correction for field contamination requires a control field. We selected a separate background field located  $15'.09$  E and  $0'.45$  N of the

central field and took another series of deep  $R$  exposures there. At this projected distance from the galaxy center, the number of M87 globular clusters is  $\lesssim 2\%$  of the level in the central field (see the wide-field GCS profiles of McLaughlin *et al.* 1994).

Finally, we took shorter series of the central field in  $V$  ( $4 \times 600$  sec) and  $I$  ( $4 \times 500$  sec) to measure the colors of the brighter globular clusters in the field. These were used to estimate the size of the GCS metallicity gradient in the core region. A summary of the observational material is given in Table 1.

Master flat fields in all three filters were constructed from a combination of dome flats and twilight exposures, and the control field was used to check that these produced globally flat calibrations to well within 1%. Absolute calibration was accomplished with  $VRI$  exposures of standard-star fields in the clusters M67, M92, NGC 4147, and NGC 7006 (Schild 1983; Christian *et al.* 1985; Davis 1990). Both nights were photometric, and images of all four standard fields were taken on each night. The zeropoints of the photometric scales in our M87 fields are judged to be uncertain by no more than  $\pm 0.02$  mag in each filter, from the observed scatter of the bright-star aperture photometry used to transfer the calibrations.

Couture *et al.* (1990) obtained  $BVI$  CCD photometry of  $\sim 270$  clusters over a roughly similar radial region around M87. Unfortunately, we cannot compare our data directly with theirs, since their field (just to the north of the M87 nucleus) has almost no overlap with ours. The much wider-field study of McLaughlin *et al.* (1994) in the  $V$  band can, however, be used for comparison since our outer zone overlaps with their inner one. For 44 objects in common brighter than  $V \simeq 22.2$ , we find  $\Delta V(\text{MHH-HHM}) = -0.035 \pm 0.014$ , confirming that there are no major zeropoint errors.

## 2.2. Photometry

To facilitate the photometry of the faint starlike objects in the central field, we first removed the background light from M87 using the ellipse-fitting codes in STSDAS. Fig. 1 shows the field after subtraction of the smooth and nearly circular isophotes. As is apparent from the figure, the model also successfully removed the bright semistellar nucleus of the galaxy, leaving only the nuclear jet, the large population of globular clusters, and a few faint background objects.

The photometry was done with the normal suite of DAOPHOT II and ALLSTAR codes (Stetson 1992) with a star-finding threshold set at  $\simeq 3.5$  times the standard deviation of the average sky noise across the frame. Two iterations of the object-finding and ALLSTAR

measurement were sufficient to capture essentially all the starlike objects on the frames, since the field is not crowded in any absolute sense. Fig. 2 shows the locations of the brighter ( $R < 23.2$ ) objects on the frame, along with the field orientation: the  $+x$ -axis is  $(32^{\circ}95 \pm 0^{\circ}5)$  eastward from due North. A  $\pm 15^{\circ}$  sector around the nuclear jet was excluded from any further analysis. A few clearly nonstellar objects (faint background galaxies) were removed objectively from the detection lists by the use of the image moment  $r_{-2}$  defined in Harris *et al.* (1991). Exactly the same rejection criteria were employed for the background field. For the magnitude range  $19.0 < R < 24.6$ , 892 starlike objects in total were measured in the central field and just 91 in the control field. Table 2 contains a partial listing of the final data, for the brightest objects: here,  $(X, Y)$  are in arcseconds relative to the center of M87, with  $X$  increasing eastward and  $Y$  northward. An electronic file of the complete data may be obtained from WEH on request.

Since the pixel-to-pixel sky noise depends dramatically on radius from the galaxy center, so does the completeness of detection at any given magnitude. (Object crowding is not important at any radius, so the completeness  $f$  is determined almost purely by the background noise). Extensive artificial-star tests were carried out to determine  $f$  and the internal precision of the photometry: scaled point-spread functions (psfs) were added to the frame, typically in groups of 200 – 300 over the entire magnitude range of interest, and then subjected to exactly the same measurement procedure as the original frame. If  $N(m)$  denotes the number of artificial stars inserted at magnitude  $m$  and  $N_{meas}$  is the number successfully recovered (at any measured magnitude), then we define  $f(m) = N_{meas}/N(m)$ .

After preliminary trials with various radial binnings, we divided the central field into four annuli as listed in Table 3 and marked in Fig. 2. The very innermost circle ( $r < 9'' \simeq 0.65$  kpc [D/15]) was eliminated from further consideration because of its overwhelmingly high background noise, which prevented any useful photometry. The results for  $f$ , in steps of 0.5 mag, are shown in Fig. 3. Note that the control field reaches significantly deeper than any part of the central field (despite its shorter exposure time) because of its much lower background light. In practice, we approximate each of the curves in Fig. 3 by the two-parameter Pritchett interpolation function (Fleming *et al.* 1995)

$$f(m) = \frac{1}{2} \left[ 1 - \frac{\alpha(m - m_0)}{\sqrt{1 + \alpha^2(m - m_0)^2}} \right] \quad (1)$$

where  $m_0$  (the “limiting magnitude” in a formal sense) is the magnitude at which  $f = 0.5$ , and  $\alpha$  measures the steepness of decline of  $f(m)$  near  $m_0$ . The fitted values of  $(\alpha, m_0)$  for each annular zone and the control field are listed in columns (3) and (4) of Table 3. Column (5) gives the total area of each zone lying within the boundaries of the central field.

The artificial-star tests were also used to evaluate the internal photometric precision, with the results shown in Fig. 4. Our limiting magnitudes  $m_0$  as listed in Table 3 correspond roughly to the levels at which the measurement uncertainty reaches  $\sim 0.25$  mag.

### 3. THE LUMINOSITY DISTRIBUTION: RADIAL TRENDS?

McLaughlin (1995) has used our HRCam data to analyze the radial structure of the inner GCS and to discuss its implications. Here, we investigate the characteristics of the GCLF (the luminosity function of the globular clusters) in the GCS core and compare it with previously published data for the outer halo.

Early studies of the GCLF in the Milky Way and M31, along with the first photometry of the brighter clusters in the Virgo elliptical galaxies, gave rise to the now-standard notion that the GCLF is roughly Gaussian in number of clusters per unit magnitude (e.g., Hanes 1977; Harris & Racine 1979; Harris 1991). On purely empirical grounds, the near-uniformity of the GCLF peak or “turnover” absolute magnitude has encouraged its use as a standard candle (Jacoby *et al.* 1992; Harris 1996b; Whitmore 1996; Kavelaars & Hanes 1997). The first photometric study that penetrated unequivocally past the turnover point in any galaxies beyond the Local Group was by Harris *et al.* (1991) for the Virgo ellipticals NGC 4472 and 4649. By now there are published studies for several other large galaxies that reach clearly fainter than the GCS turnover level and directly verify the near-Gaussian shape of the GCLF (Fleming *et al.* 1995; Whitmore *et al.* 1995; Forbes 1996a,b).<sup>3</sup>

In each of the four zones of our central field, the GCLF is defined by the number of objects remaining after (a) removal of nonstellar images by image moment analysis, (b) correction for detection incompleteness  $f$ , and (c) subtraction of the background LF, also corrected for incompleteness and normalized to the area of the zone. The results are summarized in Table 4, in 0.4-mag bins for each ring. The first column gives the central  $R$  magnitude of the bin, and the next four columns list the residual number of objects in each zone, fully corrected for incompleteness and background subtraction. For comparison, the last column gives the background LF (also corrected for incompleteness). From the relative zone areas listed in the last row, it can be seen that the background corrections are much

---

<sup>3</sup>It should be realized that the Gaussian distribution is only a convenient fitting function and has no astrophysical justification. Other equally simple analytic forms have been found that match at least as well (e.g. the  $t_5$  function of Secker 1992). As Harris (1991) points out, if the GCLF were truly Gaussian in form, then so too would be the *luminosity-weighted* luminosity function (LWLF). However, the LWLFs are decidedly *non-Gaussian* (McLaughlin 1994; McLaughlin & Pudritz 1996).

less than 10% of the GCS population in *every* zone and magnitude range except for the two faintest bins in Ring 4. Note also that we stopped the calculations in each zone when the completeness  $f$  dropped below  $\simeq 0.4$ , thus the effective limiting magnitude increases with radius.

A potential concern is that our derived LF's might be contaminated at the faint end by false detections from pure noise, particularly in Ring 1 where the background light is high. To measure this effect explicitly, we inverted the image of the central field (i.e., we reversed the sign of all the pixel values on the sky-subtracted image) and then carried out exactly the same photometric analysis on this inverted picture as on the original one (see Harris *et al.* 1991 for a more extensive description of this procedure). The detected objects on this inverted frame are all pure noise by definition. The vast majority are either fainter than our adopted limiting magnitude in that radial zone, or are rejected as nonstellar in shape, and the remaining corrections to the LF's are quite small, amounting on average to about 4 objects in the faintest bin in each zone. These corrections have been included in the final totals given in Table 4.

The GCLF's for the separate rings are plotted in Fig. 5. For rings 2, 3, and 4 the GCLF turnover (peak point) expected at  $R \simeq 23.2$  has clearly been reached and passed. The question of immediate interest is whether or not any systematic differences in the features of the GCLF show up with galactocentric distance. Standard Kolmogorov-Smirnov (K-S) two-sample tests show that rings 2, 3, and 4 are *not* significantly different from each other. This result extends that of McLaughlin *et al.* (1994), who found no variation in the GCLF over the radial range  $1'.2 \leq r \leq 6'.8$ . The same conclusion can also be drawn from attempts to fit Gaussian curves to the GCLF's, in which we find that the turnover point  $R_0$  and dispersion  $\sigma(R)$  of the fitted Gaussians are virtually identical for these three outer zones. Combining rings 2 – 4 for  $R < 23.8$ , we find by weighted least squares that the best-fit Gaussian has  $R_0 = 23.18 \pm 0.25$  and  $\sigma = 1.39 \pm 0.15$ . This fit is displayed in Fig. 6. Adding the mean color  $(V - R) = 0.50$  (see below), we obtain  $V_0(\text{turnover}) \simeq 23.7$ , in complete agreement with the values  $V_0 = 23.72 \pm 0.06$ ,  $\sigma = 1.40 \pm 0.06$  quoted by Whitmore *et al.* (1995) from an HST-based sample that reaches about half a magnitude deeper than ours.

For the innermost zone (ring 1), our data reach their reliable limit just at  $R \simeq 23.4$ , and thus we cannot make any stringent test of the GCLF turnover level except to conclude that  $R_0$  is *no brighter* there than in the outer zones. Although Whitmore *et al.* (1995) do not comment directly on this point, they also apparently did not find any strong changes in the turnover out to their radial limit of  $r(\text{max}) \simeq 114''$ . If we *assume*  $R_0 \simeq 23.2$  for ring 1 as well, then the data give a weak hint that the dispersion may be narrower there, with a best-fit  $\sigma \simeq 0.8 \pm 0.3$ . This result is indicated schematically in the lower panel of

Fig. 6. However, the relatively small sample in ring 1 prevents us from strongly ruling out a higher  $\sigma$ . A K-S test comparing ring 1 with either ring 4 or the sum of (2+3+4), over the magnitude range  $R < 23.4$ , indicates that they are different at the  $\simeq 90\%$  confidence level – again, suggestive but not definitive.

An alternate way of displaying the data to compare more readily with theory is as  $dN/dL$ , the number of clusters per unit luminosity; we call this function the LDF (HP94).<sup>4</sup> Theoretical formation models, as well as a large body of observational material for currently active star- and cluster-forming regions (e.g., HP94; McLaughlin & Pudritz 1996; Elmegreen & Falgarone 1996; Elmegreen & Efremov 1997), suggest that the initial mass distribution function of the clusters should be closely approximated by a power-law form  $dN/dM \sim M^{-\gamma}$  where the mass spectral index  $\gamma$  is typically in the range  $\sim 1.5 - 2.0$ . The LDF will have the same form as long as the mass-to-light ratio for individual clusters is independent of  $M$ .

We display the LDF in Fig. 7, for three distinct regions covering virtually the entire range of the M87 halo. Our innermost zone (ring 1) is shown as the upper set of points, covering the projected radial range  $\simeq 0.7 - 1.4$  kpc, while rings 2–4 ( $\simeq 1.4 - 10.3$  kpc) are plotted as the middle set of points. Finally, for the LDF of the outer halo, we use the  $V$ -band GCLF data of McLaughlin *et al.* (1994) covering the radial range  $2'88 - 6'82$  ( $\simeq 12.5 - 29.8$  kpc) and shown as the lower set of points.

The principal dynamical mechanism of tidal shocks should remove clusters more efficiently at lower mass and thus progressively flatten the LDF over time – and, of course, more rapidly at smaller  $R_{gc}$ . How large is this effect expected to be? The Murali & Weinberg (1997) simulations starting from a very plausible initial mass function indicate that  $\gamma$  should decrease by  $\sim 0.3$  over 10 Gyr of evolution in an M87-like core. In our data, we find that over the luminosity interval  $4.7 < \log(L/L_{\odot}) < 6.2$  (i.e., clusters more luminous than the GCLF turnover point), direct weighted fits give  $\gamma = \Delta \log N / \Delta \log L = (1.59 \pm 0.16)$  for the outer-halo zone,  $(1.65 \pm 0.17)$  for the mid-halo, and  $(1.84 \pm 0.48)$  for the inner zone. No significant differences emerge in any of the regions, and if anything, the innermost zone exhibits a *steeper* mass function. This latter result is not an artifact of increased background noise at faint magnitudes, since we explicitly measured the (small) corrections due to noise and subtracted them out (see above).<sup>5</sup> Our data, with their admitted limitations, therefore

---

<sup>4</sup>As noted by McLaughlin (1994) and McLaughlin & Pudritz (1996), the GCLF in its conventional form as number of clusters per unit *magnitude* is just the luminosity-weighted first moment of the LDF.

<sup>5</sup>The larger uncertainty on  $\gamma$  for the innermost zone is obviously a result of its much smaller sample size. Unfortunately, the sample cannot be increased, since our data already include every cluster brighter than the turnover point and within  $r \lesssim 30''$  of the nucleus. The outer-halo sample of McLaughlin *et al.* (1994) also

show no clear evidence for the trends indicated by the models.

Alternately, we might ask more specifically about the effect of dynamical evolution on the classic GCLF turnover point (plotted in its normal observational form as number per unit magnitude). The progressive removal of low-mass clusters in the inner regions, as noted above, should cause the turnover point to become brighter with time and the GCLF dispersion to become narrower. The most recent numerical simulations which deal with the GCLF (Capriotti & Hawley 1996, Vesperini 1997, Ostriker & Gnedin 1997) find that the GCLF *shape* tends to be roughly preserved as evolution continues, once it approaches its present Gaussian-like form, and that the evolution in the turnover point can be surprisingly modest. In particular, Ostriker & Gnedin (1997) predict that the cluster populations in the inner  $\sim 5$  kpc of large galaxies like M31, M87, and the Milky Way will have turnover points that are brighter by typically ( $\sim 0.3 \pm 0.1$ ) magnitude than the outer-halo populations in the same galaxies, along with narrower GCLF dispersions by typically 0.1 – 0.2 magnitude. These radial differences – both rather modest – are at least weakly consistent with our observations, which show similar turnover levels to within  $\pm 0.2$  in all of our zones, but a narrower dispersion in the innermost zone. We remark that Kavelaars & Hanes (1997) find a rather similar observational result for the Milky Way and M31: the inner-halo GCLFs are more sharply peaked, yet have turnover luminosities that are statistically indistinguishable from those in the outer halo. An earlier version of this same conclusion was found by Armandroff (1989), and the steady improvements in the Milky Way database have reinforced it.

In summary, (i) the modern theoretical simulations predict rather modest effects on the GCLF with radius (at least for the brighter part of the GCLF that is most easily observed), and (ii) our data indicate trends with radius that are, if anything, even smaller than the model predictions. The destructive mechanisms described above are important primarily on clusters *fainter* than the nominal turnover ( $\log L/L_\odot < 4.7$ , or  $M \lesssim 10^5 M_\odot$ ). Thus to find more unequivocal evidence for dynamical effects, we will need to explore the GCLF to much fainter magnitude levels and at widely separated places throughout the M87 halo. Note, however, that the deepest available study (Whitmore *et al.* 1995) shows no clear evidence for radial variations in the GCLF for  $M_V \lesssim -5.4$ , corresponding to  $M \gtrsim 3 \times 10^4 M_\odot$ .

A more extreme – and more contrived – possibility is that we are witnessing the effects of convergent evolution, in the sense that the *initial* cluster mass distribution was

---

includes the great majority of the clusters brighter than the turnover. The only experimental prospect for drawing firmer conclusions on the radial dependence of  $\gamma$  is to obtain similar observations for many more *galaxies*.

steeper in the core, and has just now reached a flatter slope which coincides with the more slowly evolving outer-halo LDF. Such an explanation seems unlikely to us particularly because it would have to apply equally well for many different types of galaxies (dwarfs, spirals, and ellipticals) within which the detailed destruction rates would differ. Also, the formation models of McLaughlin & Pudritz (1996) and Elmegreen & Efremov (1997), which successfully account for the power-law shape of the LDF, already give strong grounds for expecting that the initial LDF should be independent of galactocentric radius.

Another notable feature of Fig. 7 is the very top end of the LDF ( $\log L/L_\odot > 6$ , equivalent to  $M \gtrsim 2 \times 10^6 M_\odot$ ), which cuts off more sharply for the middle and inner zones than for the outer halo; that is, the *very* most massive globular clusters seem progressively to disappear as we move inward. Is this feature showing us evidence of dynamical friction, which is expected to become important for exactly this mass range (Tremaine *et al.* 1975; Capuzzo-Dolcetta & Tesserì 1997)? The recent simulations of Capriotti & Hawley (1996) for clusters in a large-galaxy potential predict that most of these massive clusters ( $10^6 - 10^7 M_\odot$ ) should survive if  $R_{gc} \gtrsim 20$  kpc; about half will be destroyed near  $R_{gc} \sim 8$  kpc; and almost all will disappear within  $\simeq 2$  kpc. For M87, we find from Fig. 7 that there are  $19 \pm 8$  clusters brighter than  $V \simeq 20.25$  ( $\log L/L_\odot \simeq 6$ ) in the outer zone;  $4 \pm 3$  clusters in the middle zone; and none in the inner zone. However, these numbers must be normalized to the same parent population: the total number of clusters over the range  $20.25 < V < 23.25$  is  $\simeq 650$  in the outer zone, 350 in the middle zone, and 40 in the inner zone. Thus in proportion to these totals, we would have expected to see  $10 \pm 4$  of the super-bright clusters in the middle zone if none were destroyed, but about half this many if the models are correct; we observe  $\sim 4$  in the real sample. In the inner zone, we would expect just one cluster if no dynamical destruction has occurred; we see none. Although these comparisons are only approximate ones (the radial binnings in the models are rough ones, the statistics are weak, and the observed numbers are for projected radial bins rather than true three-dimensional radii), the model predictions are consistent with the data.

Another way to state this conclusion is that, for the radial regime ( $r \gtrsim 1$  kpc) that we can most easily observe, dynamical friction has had little effect on the cluster LDF. We therefore concur with Lauer & Kormendy (1986) and McLaughlin (1995) that the GCS core radius, which is  $\gtrsim 4$  kpc, is too large to have been created by the action of dynamical friction on a hypothetical GCS that initially followed the more centrally concentrated stellar light profile (*unless* the inner clusters all formed in severely radial, plunging orbits that took them well within the stellar bulge; see Capuzzo-Dolcetta & Tesserì 1997, Capuzzo-Dolcetta & Vignola 1997. However, we regard this as a highly speculative alternative lacking any direct evidence; see the papers cited for additional discussion).

Interestingly, to detect the effects of dynamical friction on the lower-mass parts of the LDF more directly (i.e.,  $M \lesssim 10^6 M_\odot$ ), the models cited above indicate that we would have to study the cluster mass distribution within a radial regime that penetrates into the core radius of the M87 stellar *bulge* light, i.e. to within  $r \lesssim 0.5$  kpc (or about  $7''$ ). Unfortunately, there appear to be no immediate prospects for doing this: at such small radii, it is currently impossible to find and measure the fainter clusters, and there are virtually no clusters present in the first place within this small projected area. In other galaxies, the GCS populations are much smaller than in M87, and the situation is therefore even worse on observational grounds.

In conclusion, we favor the view that dynamical evolution has *not* had very dramatic effects on the shape of the GCLF for the mass range  $M \gtrsim 10^5 M_\odot$ , except possibly at the very top end ( $M \gtrsim 2 \times 10^6 M_\odot$ ) where dynamical friction may have cut off the most massive clusters within a few kpc of the nucleus. The best present observations are beginning to converge with current theoretical simulations. Still deeper measurement of the cluster population at several different places in the M87 halo would be extremely valuable, with the potential to place still more stringent limits on the dynamical models.

#### 4. COLOR AND METALLICITY DISTRIBUTIONS

The shorter exposures of the central field in  $V, I$  (Table 1) were used to measure color indices for the brighter M87 clusters and thus to investigate their metallicity distribution. The color-magnitude diagrams from our data are shown in Fig. 8. From the luminosity function of the control field (Table 4), we estimate that just 10 objects brighter than  $R \simeq 23$  should be due to field contamination, so the points plotted in these diagrams are almost entirely M87 globular clusters. The overall mean color indices of the sample (for 155 clusters brighter than  $R = 22$ ) are  $\langle V - R \rangle = 0.501 \pm 0.008$  with rms scatter  $\sigma = 0.10$  mag;  $\langle R - I \rangle = 0.617 \pm 0.011$  with  $\sigma = 0.13$  mag; and  $\langle V - I \rangle = 1.118 \pm 0.008$  with  $\sigma = 0.17$  mag. The scatter due to photometric measurement uncertainties alone averages  $\pm 0.07$  mag in each filter over this magnitude range. The intrinsic dispersion in cluster color should then be  $\sim 0.15$  mag in  $(V - I)$ , the index most sensitive of the three to metallicity.

Recently, Elson & Santiago (1996a,b) and Whitmore *et al.* (1995) have obtained HST ( $V, I$ ) photometry for samples of M87 globular clusters from three different regions in the halo. They find a distinctly bimodal color distribution – previously suspected to exist by Lee & Geisler (1993) from  $(C - T_1)$  photometry with somewhat lower internal precision – with histogram peaks at  $\langle V - I \rangle \simeq 0.92$  and  $1.23$ . These colors correspond (see below) to  $[\text{Fe}/\text{H}] \simeq -1.7$  and  $0.0$ . In addition, at high metallicities, all of the conventional photometric

indices may give systematically incorrect metallicity values (additional comments will be made on this point below). Regardless of the exact metallicities of each of the two groups, bimodal distributions of this type have the traditional interpretation that the halo formed in two major enrichment stages, involving comparable amounts of gas. Very similar bimodal distributions are clearly present in the GCSs of many giant ellipticals (e.g., Forbes *et al.* 1997; Geisler *et al.* 1996; Zepf *et al.* 1995) as well as in the Milky Way (Zinn 1985; Armandroff 1989), but may be absent, or considerably less obvious, in several other ellipticals (Ajhar *et al.* 1994; Forbes *et al.* 1996). Bimodality thus seems to be a common, but perhaps not universal, phenomenon (but see Côté *et al.* 1998).

Elson & Santiago (1996a,b) also claim the existence of a mild trend in mean metallicity with magnitude in the sense that the bluer (more metal-poor) clusters tend to be brighter. Similar trends are not obviously present in the much larger samples of clusters measured by Whitmore *et al.* (1995) or Lee & Geisler (1993), and Forbes *et al.* (1997) do not find any such effect in another giant elliptical, NGC 5846. Careful inspection of Elson & Santiago’s data (cf. Fig. 2 from their second paper) shows that their claimed trend in fact arises from an excess population of clusters in the “blue” group ( $V - I \simeq 0.92$ ) concentrated near  $V \simeq 22.0$ . This extra little clump of objects is *not* near the top end of the GCLF, despite its appearance in the Elson-Santiago diagrams; it is actually almost two magnitudes fainter than the GCLF tip.

Our sample of clusters is drawn from a parent population more than three times larger than the Elson-Santiago sample, so we should be able to make a stronger test for the reality of this feature. In Fig. 9, the mean ( $V - I$ ) color is plotted as a function of magnitude in 0.5-mag bins, extending to the faint limit of our data. Our conclusions from this exercise are that (a) the *very* brightest clusters (based on just 7 objects brighter than  $R = 20$ ) tend to fall in the “red” (more metal-rich) group; and (b) for  $R > 20$ , there is no statistically significant change in mean color with magnitude. Nevertheless, we detect the Elson-Santiago feature as a slightly bluer than average color (by 0.05 mag) at just the magnitude level that they noticed ( $R \simeq 21.5$ ,  $V \simeq 22.0$ ). In conclusion, we verify the existence of this mildly anomalous feature, but we do not find that it affects the overall structure of the GCLF in any important way. Nevertheless, their study raises the possibility of interesting fine structure in the color-magnitude diagram which should be pursued with higher precision photometry of a larger sample.

Finally, we use our ( $V - I$ ) measurements to investigate the overall *metallicity gradient* in the M87 halo. Our material, covering the inner halo, can be combined with that of Lee & Geisler (1993) for the outer halo to give us a comprehensive view of the entire galaxy. To convert ( $V - I$ ) into metallicity, we assume  $E(V - I) = 0.03$  (Burstein & Heiles 1984) for

M87 and use the conversion relation

$$(V - I)_0 = 0.18 [\text{Fe}/\text{H}] + 1.20 \quad (2)$$

which we derive from the recent database of colors and metallicities for the Milky Way clusters (Harris 1996a); it is nearly identical with earlier calibrations (Couture *et al.* 1990; Kissler-Patig *et al.* 1997), and is based essentially on the Zinn (1985) metallicity scale for the Milky Way clusters. We note in passing that these photometrically derived metallicities depend critically on the assumption that this simple linear relation is valid even at metallicities  $[\text{Fe}/\text{H}] \sim 0.0$  and higher, even though there are no Milky Way globulars with accurately measured metallicities this high. This simple assumption may not be correct and that the extrapolation of this relation may seriously overestimate the true metallicities for  $[\text{Fe}/\text{H}] \gtrsim -0.5$  (see Harris *et al.* 1992; Carretta & Gratton 1997).

Our results for the mean metallicities are listed in Table 5, for seven radial bins with  $\simeq 20$  clusters per bin: column (1) gives the mean radius of the clusters in the bin, column (2) the number of objects falling within the broad range  $0.8 < (V - I) < 1.5$ , columns (3) and (4) the mean color and the rms scatter of the sample, and columns (5) and (6) the mean metallicity and dispersion. These points are plotted in Fig. 10, in which the error bars shown are the standard deviations of the mean metallicities directly from Table 5. The *zero point* uncertainty of the  $[\text{Fe}/\text{H}]$  scale (i.e., the external error) is expected to be  $\lesssim \pm 0.25$  dex, from the  $\pm 0.03$ -mag uncertainty in the photometric zeropoint of our  $(V - I)$  scale (§2.1 above) and the similar uncertainty in the coefficients of the conversion relation Eq. (2). In Fig. 10, we also plot the Lee & Geisler (1993) metallicity measurements derived from their  $(C - T_1)$  index. Encouragingly, in the radial range of overlap between our data and theirs ( $r = 60'' - 100''$ ), the mean metallicity values agree to well within  $\pm 0.2$  dex in  $[\text{Fe}/\text{H}]$ , suggesting that the calibrations of both photometric metallicity scales are self-consistent to the level we expected.

The total range in radius covered by Fig. 10 now extends from  $10''$  to  $500''$  (or 0.7 kpc to 36 kpc). It is apparent that the *mean* GCS metallicity decreases steadily outward from  $r \simeq 60''$  to the outermost limits of the data, even though the *range* of cluster metallicities is comparably broad at any given radius (Lee & Geisler 1993; Whitmore *et al.* 1995; Elson & Santiago 1996a,b). Although the scatter of the mean points does not permit any very precise determination of the slope, the rough relation

$$[\text{Fe}/\text{H}] \simeq -0.9 \log r'' + 1.15 \quad (r > 60'') \quad (3)$$

adequately describes its systematic change. An interpretation suggested by Geisler *et al.* (1996) from their extensive analysis of the NGC 4472 GCS, which is quite similar to that of M87, is that the bimodal metallicity distribution is present at all radii and that there

is little, if any, metallicity gradient *within* either of the two subsystems. However, the metal-richer ones form a much more centrally concentrated subsystem (as they do in the Milky Way), so their relative numbers increase strongly inward and thus create the observed shift in mean metallicity with radius. Notably, however, we find that *within the GCS core radius* of  $r_c = 1' \simeq 4.3$  kpc, the mean metallicity stays constant with radius.

## 5. THE FORMATION OF SUPERGIANT ELLIPTICALS

### 5.1. M87 and the Specific Frequency Problem

The preceding discussion indicates that for M87, the inner-halo part of the GCS is simply an inward extension of the rest of the halo: the GCS in the core has a luminosity distribution function scarcely different from that of the outer halo, and the core metallicity distribution has a mean  $[\text{Fe}/\text{H}] \sim -0.3$  which would result from its being drawn primarily from the metal-richer part of the bimodal distribution, along with a smaller admixture from the metal-poor component. All the available data are quite consistent with the picture that the internal characteristics of the M87 GCS exhibit no abrupt changes with radius.

To this point, we have not yet brought in another important characteristic of the M87 system, which is the *specific frequency*  $S_N$  (Harris & van den Bergh 1981; Harris 1991), or number of clusters per unit galaxy luminosity. The specific frequency is

$$S_N = N_{GC} \cdot 10^{0.4(M_V^T + 15)} \quad (4)$$

where  $M_V^T$  is the integrated magnitude of the host galaxy and  $N_{GC}$  is the total number of globular clusters in the galaxy. It has long been realized that  $S_N$  correlates strongly with environment: the highest- $S_N$  systems are found only in some cD-type giants at the centers of rich galaxy clusters (Harris *et al.* 1995; Blakeslee 1997 [hereafter B97]), while the sparsest globular cluster populations usually reside in “field” or small-group ellipticals in lower-density environments (Harris 1991; West 1993). Thus to develop a larger picture of the origin of the GCS, we must also connect M87 to similar central-giant ellipticals in other clusters. We now turn to this somewhat broader issue.

We first provide an improved calibration of  $S_N$  for M87, by combining our new data with the wider-field counts of McLaughlin *et al.* (1993, 1994) and Harris (1986). McLaughlin *et al.* find  $3100 \pm 130$  clusters brighter than  $V = 24$  over projected radii  $1'.97 \leq r \leq 9'.09$ , while the GCS radial profile of McLaughlin (1995) from our HRCam data gives  $1300 \pm 80$  clusters brighter than  $V = 24$  and within  $r = 1'.97$ . For the GCLF parameters adopted above ( $\sigma = 1.4$ ,  $V_0 = 23.7$ ), the globulars brighter than  $V = 24$  account for  $58\% \pm 6\%$  of the

whole population; thus, the total number of M87 clusters with  $r \leq 9'.09 = 39.7(D/15)$  kpc is  $7590 \pm 1050$ . Then from the M87 surface photometry of de Vaucouleurs & Nieto (1978), we find that the integrated magnitude of the galaxy interior to  $r = 9'.09$  is  $M_V = -22.3$  [for  $(B - V) = 1.0$  and  $(m - M)_V = 31.0$ ]. The *metric specific frequency* of M87, which is defined by B97 as the ratio of cluster numbers to galaxy light inside  $r = 40$  kpc, is then

$$S_N^{40}(M87) \simeq (7590 \pm 1050) \times 10^{0.4(-22.3+15)} = 9.1 \pm 1.3 . \quad (5)$$

The number density of globular clusters in M87 falls off more gradually with  $r$  than does the intensity of background galaxian light (Harris & Smith 1976; Harris 1986; McLaughlin *et al.* 1993), so the specific frequency must increase with galactocentric radius and the global  $S_N$  of the entire galaxy necessarily exceeds  $S_N^{40}$ . To estimate the former quantity, we adopt  $r = 25' = 109(D/15)$  kpc as the “edge” of the galaxy (which has a total magnitude of  $M_V^T = -22.43$ ; de Vaucouleurs & Nieto 1978) and of the GCS. The observed surface density profile of the outer cluster system can be taken from the wide-field counts of Harris (1986); these show that the cluster population beyond  $9'$  makes up  $(1.048 \pm 0.081)$  times the sum from  $r = 2'$  to  $9'$ . The total number of clusters over all radii and magnitudes is then  $13200 \pm 1500$ , and hence

$$S_N(M87) = 14.1 \pm 1.6 . \quad (6)$$

The main source of uncertainty is the behavior of  $\sigma_{cl}$  in the outermost halo of M87.

The global specific frequencies of other elliptical galaxies in Virgo are typically of order  $S_N \sim 5$  (Harris 1991). A valuable template for a ‘normal’ galaxy in this respect is M49 = NGC 4472, which is comparable to M87 in brightness and size, but which has a global  $S_N = 6.0 \pm 1.5$  and a metric  $S_N^{40} \simeq 4 \pm 1$  (from the data of Harris 1986). Over all types of environments,  $S_N$  for E galaxies ranges from a minimum below  $S_N \sim 1$  in some field ellipticals up to  $\gtrsim 15$  for the richest cD’s. The underlying cause for this amazingly wide range among otherwise similar galaxies has been rather a mystery since the phenomenon first became clear two decades ago (e.g., van den Bergh 1977; Harris & Petrie 1978; Harris & van den Bergh 1981).

## 5.2. Scaling Relations for Brightest Cluster Galaxies

The search for an empirical set of necessary *and sufficient* conditions for high  $S_N$  has been a long one. While the highest- $S_N$  galaxies often have a cD morphology, and are always the central members of their parent clusters or subclusters, there are many other cD and brightest cluster galaxies (BCGs) with quite normal GCS populations (e.g., McLaughlin

*et al.* 1994; Harris *et al.* 1995). However, the recent work of B97 and Blakeslee *et al.* (1997) (hereafter BTM97) considerably enlarges the database of GCS properties for these galaxies. Blakeslee *et al.* show that  $S_N^{40}$  in the BCGs is correlated with several indicators of the total cluster mass, such as the velocity dispersion of the galaxies and the X-ray luminosity of the hot gas residing in the cluster potential well. Moreover, it is now apparent from the BTM97 study that *BCGs cover a smooth continuum* of specific frequency values, from normal levels up to the most extreme known.

First we collect the available data for these BCGs. BTM97 give the “metric”  $S_N^{40}$  values for BCGs in 19 Abell clusters, measured by their surface brightness fluctuation technique. In addition, Harris *et al.* (1995) give global  $S_N$  values for other BCGs measured by direct resolution of the GCS population. From seven galaxies measured through both techniques (NGC 1399, 3842, 4486, 4874, 4889, 6166, and 7768), we derive a mean ratio  $\langle S_N/S_N^{40} \rangle = 1.3 \pm 0.2$  which can be used to convert approximately between these two quantities in cases where only one has been measured. In Table 6, we summarize the updated parameters for 11 centrally dominant giant E galaxies in clusters not listed by BTM97. Here, columns (1) and (2) give the galaxy name and host cluster; column (3) the total luminosity of the BCG (assuming  $H_0 = 80 \text{ km s}^{-1} \text{ Mpc}^{-1}$ ); columns (4) and (5) the global and metric specific frequencies; column (6) the velocity dispersion  $\sigma_{cl}$  of the galaxies in the cluster; and column (7) the X-ray temperature of the hot ICM gas in the cluster. Reference sources are listed in parentheses in columns (6-7). Adding them to the Blakeslee sample, we now have a total of 30 BCGs spanning the entire range from quite sparse groups (Leo, Centaurus) all the way up to the richest types of Abell clusters.<sup>6</sup>

The basic difference between the BCGs and other E galaxies is shown graphically in Fig. 11. Here, the total population of the GCS (calculated from the global  $S_N$  and the galaxy luminosity) is plotted against  $M_V^T$ . A total of 82 elliptical galaxies are now included in this plot; data for the non-BCG systems are taken from the compilations of Harris & Harris (1998) and Durrell *et al.* (1996) with a few more recent updates from the literature. Despite the significant scatter, it is clear that to first order,  $N_{GC}$  is directly proportional to galaxy luminosity (that is,  $S_N \simeq \text{constant}$ ) over a range of more than  $\sim 10^4$  in  $L_{gal}$ . However, *for the BCGs alone,  $S_N$  is itself a function of galaxy size*, increasing steadily toward larger and more massive systems.

As is clearly shown by B97 and BTM97, BCG specific frequency also increases

---

<sup>6</sup>In a few cases, the BCG is actually not the optically brightest galaxy in the cluster (Virgo and Coma are well known examples in which another cluster elliptical is slightly more luminous than the central one). Here, we are using the term “BCG” specifically to mean the *centrally located* giant E galaxy in the cluster.

with total cluster mass (represented either by the velocity dispersion  $\sigma_{cl}$  or the ICM gas temperature  $T_X$ ). In Fig. 12 we show  $S_N$  versus  $T_X$  for our augmented sample of BCGs, and Fig. 13 is a similar plot of  $S_N$  and  $N_{GC}$  versus  $\sigma_{cl}$ . The overall dispersion of points in both graphs shown here – as well as the several others shown in BTM97 – is larger than for the Blakeslee sample by itself. Nevertheless, the general trend remains that more populous GCSs *and* higher specific frequencies are found in galaxy clusters with systematically higher mass, deeper potential wells, and hotter and more massive ICMs. Probably the clearest representation of these trends appears in the plots against  $\sigma_{cl}$ . As did BTM97, we adopt  $\sigma_{cl}$  as the primary indicator of the size of the cluster, and using this, we can derive several simple *empirical scaling relations* for specific frequency, total GCS population, and BCG luminosity. Least-squares solutions against cluster velocity dispersion give the following:

$$\log S_N = (0.71 \pm 0.26) \log \sigma_{cl} - (1.11 \pm 0.68), \quad (7)$$

$$\log N_{GC} = (1.58 \pm 0.32) \log \sigma_{cl} - (0.42 \pm 0.86), \quad (8)$$

$$\log (L_{gal}/L_{\odot}) = (0.86 \pm 0.19) \log \sigma_{cl} + (8.55 \pm 0.51), \quad (9)$$

where  $\sigma_{cl}$  is in  $\text{km s}^{-1}$ . In other words, we have approximate scaling laws  $N_{GC} \sim \sigma^{1.6}$ ,  $L \sim \sigma^{0.9}$ , and  $S_N \sim N/L \sim \sigma^{0.7}$ . (We ascribe no particular significance to the fact that these correlations all pass through  $(0, 0)$ ; at the low-mass end, all these relations require downward extrapolations which are not constrained by our data.) These relations stand independently of any of the theoretical hypotheses that will be discussed below.

Much of the scatter in all these correlations may simply be due to the sizable measurement uncertainties in the individual  $S_N$  values. Only two objects stand out as genuinely anomalous: these are NGC 1399 (a high- $S_N$  but low-luminosity cD in the relatively low-mass Fornax cluster), and NGC 1275 (the extremely luminous but *low*- $S_N$  central cD in the massive Perseus cluster). The populous GCS in NGC 1399 has been measured several times with highly consistent results (Hanes & Harris 1986; Bridges *et al.* 1991; Kissler-Patig *et al.* 1997, among others), and the galaxy’s luminosity profile is well enough established (e.g. Killeen & Bicknell 1988) to permit accurate calibration of either  $S_N^{40}$  or  $S_N(\text{global})$ . NGC 1399 is a challenging anomaly in almost any formation scenario. In the case of NGC 1275, the central galaxy is clearly extremely luminous even after accounting for the recent star formation present there, and the GCS is just as clearly unexceptional (Kaisler *et al.* 1996). NGC 1275 might plausibly be explained by supposing that the Perseus cluster is a rare instance where the central cD built up from an initially rather normal E galaxy through amalgamation with many neighboring galaxies, as discussed by Kaisler *et al.*

### 5.3. Evolutionary Scenarios

How did these intriguing BCG systems arise? The ideas that have developed in the literature can be grouped into three main approaches: (1) the high- $S_N$  galaxies acquired large numbers of “extra” globular clusters in various possible ways long after their initial formation stage; or (2) the high  $S_N$  is a form of optical illusion, in which a population of intergalactic globular clusters that simply occupy the potential well of the cluster as a whole lies at the same location as the BCG; or (3) the GCS populations were largely built in at birth, with later minor adjustments. In the next three sections, we discuss each of these options in turn. A key to keep in mind is that any proposed solution to the  $S_N$  problem must explain not only the sheer total number of clusters present in these galaxies; it must also address several other measurable GCS characteristics including their spatial distribution, velocity distribution function, and metallicity distribution function. As yet, no complete model has been developed which can quantitatively deal with all these aspects of the problem. To help evaluate the various options, we first comment on the evolutionary scenarios.

Among the proposed mechanisms for supplementing the GCS populations of dominant cluster galaxies relatively late in their lives are the following:

(1) Cooling flows: M87 and other cD galaxies have extended coronae holding large amounts of hot low-density gas, and it has been hypothesized that globular clusters somehow actively form out of the ongoing cooling flow from this gas, thus adding to the original cluster population (Fabian *et al.* 1984). However, this model fails on several grounds to predict the quantitative features of the observed GCSs in these galaxies, such as the cluster metallicity distribution; the complete lack of correlation between GCS population and cooling-flow amplitude; the near-complete absence of any young, massive star clusters in most cooling-flow galaxies; and the large velocity dispersion in the GCS which is unlike that expected from objects condensing out of a cooling flow (see Grillmair *et al.* 1994b; Harris *et al.* 1995; Kaisler *et al.* 1996; Bridges *et al.* 1996; Holtzman *et al.* 1996).

(2) Stripping from other galaxies: the possibility that central BCGs might have acquired halo globulars from other, *fully formed* galaxies during close encounters was explored in a series of models by Muzzio and collaborators (see Muzzio 1987 for a review). These investigations showed that cluster swapping may be responsible for minor rearrangements of clusters between galaxies, but is unable to produce the major increases in  $S_N$  (factors of 2 to 3) that we need for the central cD galaxies. A related possibility, in which tidal debris from systems throughout a galaxy cluster sinks onto a BCG at the bottom of the potential well (again, after the main epoch of galaxy formation), is discussed and rejected by McLaughlin *et al.* (1994).

Another version of this approach, pointed specifically at explaining the bimodal metallicity distributions seen in giant elliptical GCSs, has recently been developed by Côté *et al.* (1998). They assume that a typical giant elliptical such as NGC 4472 started as a ‘seed galaxy’ of smaller size, and has since absorbed large numbers of smaller (mostly dwarf) galaxies. The metal-richer globular clusters in the final gE are thus mostly ones that formed with it originally, while the metal-poorer clusters are the ones acquired from the accreted dwarfs. By quantitative numerical simulations, Côté *et al.* show that a plausible range of GCS metallicity distributions can be accounted for this way. To account for a much higher- $S_N$  BCG like M87, they assume further that the giant central galaxy accretes only the high- $S_N$  envelopes of the smaller galaxies orbiting in the potential well of the galaxy cluster, without absorbing the central (cluster-poor) cores of those galaxies. The advantage of this general scheme is that it employs a process (small-galaxy accretion and harassment) which must surely happen at some level in almost any rich environment like Virgo, Fornax, or Coma. However, some related worries are that (i) to explain the *entire* GCS metallicity distribution function this way, it is necessary to assume that very large numbers of small galaxies are accreted (many hundreds for a case like NGC 4472, and even more for M87); (ii) if (typically) half the light of the gE is from smaller, accreted, and more metal-poor systems, they should not have the high ( $\sim$  solar or higher) mean metallicities that they are observed to have; and (iii) an environment like Virgo should contain hundreds (perhaps thousands) of stripped cores of dwarf galaxies whose envelopes were accreted by the central BCG. These expectations run counter to the available observations. Nevertheless, their discussion correctly calls for additional investigation through detailed N-body simulations.

(3) Mergers: E galaxies can be built out of the collisions and mergers of disk galaxies, and massive globular-like star clusters can form in the shocked gas during the merger (Schweizer 1987, 1997; Kumai *et al.* 1993a). The newly formed clusters may end up in a more centrally concentrated and more metal-rich subsystem than the original (metal-poor, spatially extended) GCSs of the colliding galaxies (Ashman & Zepf 1992; Zepf & Ashman 1993). Several galaxies in which this process is actively happening have now been identified (e.g., Holtzman *et al.* 1992; Whitmore *et al.* 1993b; Whitmore & Schweizer 1995; Holtzman *et al.* 1996; Miller *et al.* 1997). It is important to keep in mind that the specific frequency of the merged remnant may end up *either* larger or smaller than in the pre-merger galaxies, depending on factors such as the total amount of incoming gas, the collision geometry, and (most importantly) the efficiency of cluster formation relative to field-star formation.

The merger mechanism is arguably quite a plausible way to build ellipticals that end up with low-to-normal  $S_N$  (Harris 1981, 1995; Miller *et al.* 1997), since typical disk galaxies have relatively few halo clusters of their own, as well as modest supplies of gas. For example, isolated E Galaxies such as NGC 3557 (Morbey & McClure 1985) and NGC 720

(Kissler-Patig *et al.* 1996), which have elongated shapes and very low specific frequencies in the range  $S_N \lesssim 2$ , are prime candidates to be the results of disk-galaxy mergers that happened long ago. The more recent merger remnants such as NGC 3921 (Schweizer *et al.* 1996) and NGC 7252 (Miller *et al.* 1997) appear to be evolving into the same type of elliptical, with modest populations of globular clusters and  $S_N \sim 2 - 3$ , as predicted by Harris (1995). However, applying the same model to giant ellipticals at the highest end of the  $S_N$  scale leads to much more serious difficulties. For such galaxies, thousands of massive star clusters would have to be formed during the mergers, requiring an enormous input supply of gas – so large, in fact, that the merging “galaxies” must in essence be pregalactic clouds (Harris 1995). In addition, some high- $S_N$  galaxies do not have clearly bimodal GCS metallicity distributions; the highest- $S_N$  systems do not have the lowest radial metallicity gradients; and the lower-metallicity clusters in these gE’s are often not as metal-poor as those in spirals. All of these points – and others raised in the references cited above – speak against the merger model as a viable origin for the extreme BCGs (Geisler *et al.* 1996; Forbes *et al.* 1997).

In summary, these secondary-evolution processes appear able to produce measurable changes in  $S_N$  for ellipticals with cluster populations in the low or normal range. However, for M87 and the other supergiant cD galaxies with the highest specific frequencies, no viable production mechanisms have convincingly emerged from these approaches.

#### 5.4. Intergalactic Globular Clusters

White (1987) suggested that clusters of galaxies might host populations of globular clusters that are not currently bound to any one galaxy, but instead move freely in the potential well of the cluster as a whole. West *et al.* (1995) have revived this idea, and cite what is essentially a version of Blakeslee’s (1997) correlation between BCG specific frequency and galaxy cluster X-ray luminosity as possible evidence for the existence of these intergalactic globular clusters (IGCs). In their scenario, the  $S_N$  of a central BCG could be artificially enhanced by the superposition of IGCs — which would naturally have their largest space density in the very core of the cluster — on top of a normal ( $S_N \sim 5$ ) population of globulars that actually are bound to the BCG. Indeed, given the existence of diffuse light in galaxy clusters (e.g. Coma: Thuan & Kormendy 1977), and the recent identification of candidate intergalactic stars in Fornax (Theuns & Warren 1997) and Virgo (Arnaboldi *et al.* 1996; Ferguson *et al.* 1996; Mendez *et al.* 1997; Ciardullo *et al.* 1998), it would be surprising if IGCs do *not* exist. However, the question whether a population of IGCs could *single-handedly* give rise to the high- $S_N$  phenomenon is rather a different

matter.

In our view, and as discussed by White (1987), *any IGCs should be found only in association with diffuse cluster light from intergalactic stars*. That is, we consider it highly unlikely that globular clusters preferentially condensed out of the hot, diffuse gas that pervades galaxy clusters, leaving no other form of stellar material. Furthermore, to generate a high  $S_N$  in the central galaxy, this IGC component must itself have (as we will see quantitatively below) an extremely high and nonuniform  $S_N$ . A plausible origin for this component of an intracluster medium could be from the stripping of material from young, gas-rich galaxies *during* the collapse of a cluster (see also Merritt 1984), at an early enough stage that many galaxies had formed globular clusters but had yet to produce most of their halo field stars. Most of the residual gas in these young galaxies would then have been heated to the virial temperature of the surrounding cluster and joined the ICM which, in large clusters, outweighs the stellar material in the galaxies (David *et al.* 1990; Arnaud *et al.* 1992; Whitmore *et al.* 1993a). This option is worth investigating in some detail, since it stands potentially to address, at once, the issues of BCG specific frequency, diffuse light in galaxy clusters, and cD envelope formation.

The first problem is to account for a correlation between cluster X-ray luminosity and the specific frequency of the intergalactic stellar material (and hence for the correlations of West *et al.* and B97). Let us define a globular cluster formation efficiency

$$\epsilon \equiv \frac{N_{GC}}{M_{stars} + M_{gas}} , \quad (10)$$

where  $M_{stars}$  is the mass in the stellar component of the galaxy and  $M_{gas}$  is the mass of the leftover gas unused for star formation. We can then write the presently observed specific frequency as

$$S_N \propto \frac{N_{GC}}{M_{stars}} = \epsilon \left( 1 + \frac{M_{gas}}{M_{stars}} \right) . \quad (11)$$

Suppose now that  $\epsilon$  is basically similar from place to place (see HP94; we will also use this assumption in the next section). Then, any galaxies in which star formation proceeded nearly to completion ( $M_{gas}/M_{stars} \ll 1$ ) would end up with essentially equal (and normal)  $S_N$  set by the value of  $\epsilon$ . However, many slow-forming, late-type galaxies could well have been destroyed at a point in their lives when  $M_{gas}$  was still large. The stars and globular clusters from these shredded gas-rich objects would also have spilled into the cluster at large, producing an  $S_N$  larger than normal by a factor  $\sim (1 + M_{gas}/M_{stars})$ . In absolute terms, we could suppose that the collapse of more massive galaxy clusters engendered the destruction of larger numbers of gaseous systems, thus leaving behind larger ratios of gas mass to total stellar mass, as is observed (David *et al.* 1990; Arnaud *et al.* 1992). As

well, this effect could contribute to the growth of cD envelopes and the establishment of a correlation between cD envelope luminosity and the X-ray luminosity  $L_X$  of the surrounding cluster gas (Schombert 1988; López-Cruz *et al.* 1997).

Pursuing this option, let us now assume that a population of IGCs with specific frequency  $S_N^{IGC}$ , and an envelope composed of diffuse intracluster light  $L_{env}$ , are superimposed on a BCG body with normal  $S_N^{body}$ . The apparent specific frequency of the combination will be

$$S_N^{tot} = \frac{S_N^{body} + (L_{env}/L_{body})S_N^{IGC}}{1 + L_{env}/L_{body}} . \quad (12)$$

Since  $S_N^{IGC} > S_N^{body}$  by hypothesis, the addition of the IGC component will increase  $S_N^{tot}$ .  $L_{env}/L_{body}$  increases weakly with the parent cluster  $L_X$  (Schombert 1988). Thus,  $S_N^{tot}$  would increase with  $L_X$  even if  $S_N^{IGC}$  were constant from cluster to cluster. However,  $S_N^{tot}$  in cD galaxies should then also correlate with the relative size of their cD envelope,  $L_{env}/L_{body}$ . This is *not* an observed trend (for example, M87 itself has a rather modest envelope but one of the highest and best-measured specific frequencies; and other BCGs with very massive envelopes such as NGC 6166 have unexceptional  $S_N$  values; see the next section).

The alternative is to let  $S_N^{IGC}$  also increase with cluster  $L_X$  (or mass, or velocity dispersion, or temperature). By Eq. (11), this will occur if the formation of more massive galaxy clusters somehow involves the destruction of protogalaxies with systematically larger gas fractions  $M_{gas}/M_{stars}$ . In this case, the initial metallicity of the intracluster gas should be *anti*-correlated with  $L_X$  (see also David *et al.* 1990). Even though some subsequent contamination due to galactic winds from the surviving protogalaxies must certainly have occurred (e.g., Matteucci & Gibson 1995), such an anti-correlation does appear to exist (Fabian *et al.* 1994). Thus, this scenario would allow IGCs to resolve at least some aspects of the high- $S_N$  problem if we allow  $S_N^{IGC}$  to increase with cluster mass. Unfortunately, this descriptive scenario cannot account *quantitatively* for other features of the GCS, as we will see next.

Let us try to construct a model for M87 specifically, by building it from an M49-like body with a normal GCS, surrounded by a much more extended IGC envelope. In Fig. 14 we model the observed  $B$ -band surface photometry of M87 (Carter & Dixon 1978) as the sum of two components. One is the underlying body of the galaxy, with a conventional  $r^{1/4}$  law profile,

$$\mu_B^{body} = 14.615 + 2.658 (r/\text{arcsec})^{1/4} \text{ mag arcsec}^{-2} . \quad (13)$$

The other is a faint envelope which, for the sake of our argument, is assumed to be part of the intracluster medium around M87:

$$\mu_B^{env} = 26.675 + 1.875 \log [1 + (r/1200'')^2] \text{ mag arcsec}^{-2} . \quad (14)$$

The envelope necessarily has a very large core radius of  $24'.7 \simeq 108(D/15)$  kpc. Beyond this core radius, the envelope light behaves roughly as  $I_{env} \propto r^{-1.5}$ . We note that Carter & Dixon (1978) find an especially bright and extensive envelope component by comparison with de Vaucouleurs & Nieto (1978) or other authors; thus, our two-component model is a “maximal-envelope” solution.

Integration of Eqs. (13) and (14) shows that in the radial regime  $1' \lesssim r \lesssim 6'.5$ , over which Cohen & Ryzhov (1997) have recently obtained high-quality radial velocities for 205 globular cluster candidates in M87, the envelope contributes to the total light of the galaxy in the ratio  $L_{env}/L_{body} \sim 0.10 - 0.15$ . The total specific frequency of M87, averaged over this same interval, is roughly  $S_N(\text{M87}) \sim 11$ , while that of M49 (which we shall take to represent the underlying  $S_N^{body}$  of M87) is  $\sim 4.7$ . Thus the fraction of the globulars around M87 that are actually bound to it would be

$$\frac{N_{body}}{N_{tot}} = \frac{S_N^{body}}{S_N^{tot}} \left( 1 + \frac{L_{env}}{L_{body}} \right)^{-1} \sim 0.4, \quad 1' \lesssim r \lesssim 6'.5. \quad (15)$$

The globulars bound to the galaxy will have a Gaussian velocity distribution with an intrinsic dispersion  $\sigma_v \sim 270 \text{ km s}^{-1}$  characteristic of the stellar core of the galaxy (e.g. Sembach & Tonry 1996), while the IGCs that are spatially superimposed will have  $\sigma_v \sim 570 \text{ km s}^{-1}$  typical of the early-type galaxies in Virgo (Binggeli *et al.* 1987). The combination of the two, in the proportions given by Eq. (15), can be reasonably well described by a Gaussian with  $\sigma_v \sim 400 \text{ km s}^{-1}$ , which is not inconsistent with the data of Cohen & Ryzhov (1997). However, the most noticeable effect of any IGCs would show up in the wings of the velocity distribution: the Cohen-Ryzhov sample of 205 globulars built in these proportions should have  $\sim 5$  clusters with  $v > 1000 \text{ km s}^{-1}$ , whereas the actual sample has none.

A still more stringent test comes from the decomposition of the M87 surface brightness, together with the observed specific frequency, into putative “body” and “envelope” (IGC) components. Suppose that the body of M87 has a specific frequency profile  $S_N^{body}$  identical to that of our ‘template’ galaxy M49 (shown in Fig. 15, along with the total  $S_N^{tot}$  observed for M87). *By hypothesis*, the difference between  $S_N^{tot}$  and  $S_N^{body}$  is due to the intergalactic envelope, which allows us to find  $S_N^{IGC}$  as a function of  $r$ . The results of this exercise are shown in Fig. 15b as the solid dots. The open squares in the same figure show the  $S_N^{IGC}$  that is inferred if the “body” of M87 is assumed instead to have  $S_N = 5$  throughout, with no dependence on galactocentric radius.

The implications of this exercise are severe. In particular, we find that  $S_N^{IGC} \propto r^{-1 \pm 0.25}$  between  $r \simeq 1'.2$  and  $r \simeq 9'$  ( $\simeq 5$  to  $40$  kpc). Because the cD envelope, or diffuse cluster light, has an essentially constant surface brightness at these radii (see Fig. 14), this means that  $S_N^{IGC}$  is directly proportional to the projected number density  $\sigma_{IGC}$  of the supposed

intergalactic globulars; thus, we conclude that  $\sigma_{IGC} \propto R_{gc}^{-1 \pm 0.25}$ . That is, we are forced to claim that the intergalactic clusters are significantly concentrated towards the center of the galaxy itself, *with a core radius no larger than  $\sim 1' = 4.3 \text{ kpc}$*  (that is, the same core radius as the M87 GCS itself). Such behavior is unacceptable for any collection of truly intergalactic objects, and completely contradictory to our original hypothesis. It is also worth noting that the deduced absolute value of  $S_N^{IGC}$  reaches a level in the core ( $> 100$ ) that is an order of magnitude larger than in any known galaxy.

We might try to get around the strong radial dependence of the IGC cluster component by assuming an  $S_N^{IGC}$  that is independent of galactocentric radius, and then use this and the observed  $S_N^{tot}$  and  $S_N^{body}$  to solve for the ratio  $L_{env}/L_{body}$ . The observed total surface-brightness profile of M87 can then be used to find the envelope intensity  $I_{env}$  as a function of  $r$ . However, this rather desperate argument results in a diffuse light component that varies essentially as  $I_{env} \propto r^{-1}$  down to  $\sim 1'$  distances from the center of M87 – which again implies that this “intergalactic” material must in fact be bound to the galaxy. Finally, we note also that if we had used the de Vaucouleurs & Nieto (1978) photometry instead, the solution for the envelope (Fig. 14) would have been considerably fainter,  $S_N^{IGC}$  even larger, and thus even less favorable to the scenario.

It is important to emphasize more descriptively why the IGC model fails. The key is that the “specific frequency problem” embodied by M87 is a *local* problem everywhere in the halo as well as a *global* one. M87 has an anomalously large cluster population at all galactocentric radii  $r$  and not just in its cD envelope. Thus, for example, we cannot turn M49 into M87 simply by adding large numbers of extra clusters to its outskirts; they must be added in the same proportions all the way in to the inner halo and core of the galaxy as well (Harris 1986). This requirement then forces the postulated IGC profile to have a central concentration resembling the underlying galaxy, as well as an inordinately high specific frequency. There appears to be no natural way to do this through the IGC model, because a realistic IGC component, or a population of clusters tidally stripped and accreted from other galaxies, would preferentially boost the cluster population in the outer halo of the galaxy while leaving the inner halo relatively unchanged.

The argument we have just outlined may, however, not apply to all high- $S_N$  BCGs. Some other BCGs have relatively much larger cD envelopes and thus, probably, stronger contributions from the central cluster potential well. The intriguing case of NGC 1399, the BCG in the Fornax cluster, may represent one such situation. Recent kinematic studies of its GCS (Kissler-Patig 1998; Minniti *et al.* 1998) show that for radii  $\gtrsim 20 \text{ kpc}$  the velocity dispersion of its globular clusters matches the surrounding Fornax galaxies rather than the NGC 1399 halo light (a difference of a factor of two in  $\sigma(v_r)$ ). We are clearly just beginning

to understand how these rather unusual galaxies were built.

### 5.5. A Formation Scenario

The preceding arguments favor the view that the essential features of the M87 GCS, and the other high- $S_N$  cD systems like it, were built in at very early times. Somewhat by default, this “initial conditions” route has usually relied on the supposition that the *efficiency of globular cluster formation*  $\epsilon$  as defined in Eq. (10) could have differed by about one order of magnitude *ab initio* among E, cD, dwarf, and spiral protogalaxies, thus directly creating the large range in  $S_N$  that we now see (e.g., Harris 1981, 1991; van den Bergh 1984; HP94). It is possible that the amount of gas cloud shocking and turbulence could have directly governed  $\epsilon$ , driving it up to higher values in denser or more massive protogalactic environments where collision speeds were higher. Unfortunately, to date this has been a somewhat *ad hoc* view with little observational evidence that could be brought to bear one way or the other, and so it, too, has been a less than satisfactory option.

The recent work of B97 and BTM97 opens the door to an alternate approach to this problem. Their data (see above) imply more clearly than before (see West 1993 and Kumai *et al.* 1993 for similar earlier suggestions) that  $S_N$  increases with the overall mass density of the protogalactic environment. B97 proposes essentially that the high- $S_N$  galaxies do not have excess numbers of clusters; instead, they have artificially low total luminosities relative to their globular cluster populations. In this picture, the “missing light” is in the hot intracluster gas that never formed stars.

In such a scenario, then it is natural to ask why this gas was unused for star formation, and how it ended up where it did. The earliest  $\sim 1$  Gyr history of an E galaxy is expected to be heavily influenced by the SNII supernova rate from the first generation of massive stars, and the subsequent development of a galactic wind (Mathews & Baker 1971; Larson 1974; see Loewenstein & Mushotzky 1996 or Gibson 1994, 1996, 1997 for recent overviews). Under the right conditions a large fraction of the original protogalactic gas can be ejected outward by the wind to join the ICM. It seems highly likely to us that galactic winds would have influenced the GCS specific frequency, and by different degrees in different galaxies. Our reason for proposing this is based primarily on the timing of the GCS formation epoch: a large protogalaxy should accumulate from many smaller ( $10^8 - 10^9 M_\odot$ ) dwarf-sized gas clouds (supergiant molecular clouds or SGMCs), which provide the right host environments for globular cluster production (Searle & Zinn 1978; Larson 1990b, 1993; HP94). In this picture, we postulate that each SGMC contains several *protocluster cores*, which are the much denser sites where star formation can take place at the necessary  $\gtrsim 50\%$  efficiency

to produce a bound star cluster. Since the protocluster cores are expected to build up over timescales  $\sim 10^8$  y out of the gas in SGMs (HP94; McLaughlin & Pudritz 1996; Elmegreen & Efremov 1997), it is likely that they would form very early in the evolution of the protogalaxy, before the lower-density majority of the gas began star formation in earnest. Thus, the globular clusters should already be present before the wind reaches its peak at a few  $\times 10^8$  y and interrupts subsequent field-star formation.

In essence, we suggest that *for normal E galaxies* with specific frequencies  $S_N \lesssim 5$ , the early galactic wind did *not* eject large amounts of the original gas supply. Today, these galaxies have GCS specific frequencies fairly close to the original cluster formation efficiency. However, in systems like M87, we propose that the galactic wind was stronger, ejecting much of the original gas mass outward into the dark-matter potential well of the surrounding cluster, and leaving behind a GCS with an artificially high  $S_N$ .

Is this idea a realistic one for gas within such massive potential wells as we find in the BCGs? (Normally, we would expect the *less* massive protogalaxies to be able to eject higher proportions of their initial gas.) Gibson (1997) provides a comprehensive discussion of the way that various parameters affect the SNII production and mass ejection rate. Effective ways to increase the amount of mass loss are (a) to increase the star formation efficiency factor  $\nu = \dot{M}_\star/M_{tot}$ , which would boost the early supernova rate; or (b) to decrease the rate at which the expanding supernova remnants can cool radiatively and lose energy; or (c) to adopt an IMF flatter than the normal Salpeter ( $x = 1.35$ ) slope, thus increasing the number of Type II SNe per unit mass. Other studies have suggested that an IMF slope  $x \simeq 1$  is also appropriate for matching the observed Fe and O abundances in the ICM gas (e.g. Loewenstein & Mushotzky 1996; Arimoto & Yoshii 1987; Renzini *et al.* 1993; David *et al.* 1991, among others). We are, however, looking for a way to generate a *difference* in the mass loss rate (and hence  $S_N$ ) in a BCG like M87, compared with normal systems like M49. Given that these galaxies have rather similar compositions and structures, we see no compelling reasons to suggest arbitrary differences in the SNR cooling rates, or the IMF. Thus of the various options mentioned above, the most plausible appears to us to be the star formation rate  $\nu$ . Our scenario therefore boils down to the suggestion that BCGs had an extraordinarily high  $\nu$  at early times.

Another important point to consider is that the simple one-zone wind models mentioned above are an oversimplification for large protogalaxies, which were likely to have been highly clumpy. Thus the parametrizations of mass loss rates for monolithic models such as the ones reviewed by Gibson (1997) should not be taken too literally. For a central supergiant like M87, which is at the gravitational center of its surroundings, the protogalaxy would have been the site of a considerable amount of gas infall and chaotic, violent motion which

could have encouraged early, rapid star formation and a more massive SNII-driven wind. This picture is consistent with the considerable evidence that many large E galaxies almost certainly formed at epochs predating  $z \sim 3$ , and some probably began major star formation at  $z \gtrsim 5$  (e.g., Larson 1990a; Maoz 1990; Turner 1991; Whitmore *et al.* 1993a; Loewenstein & Mushotzky 1996; Mushotzky & Loewenstein 1997; Steidel *et al.* 1996; Giavalisco *et al.* 1996; Bender *et al.* 1996; Ellis *et al.* 1997, to name a few; see also HP94 for a timing argument in support of a redshift  $z \gtrsim 5$  for the first epoch of globular cluster formation).

We emphasize again that we are not suggesting this approach as the way for a *typical* galaxy (elliptical or spiral) to form. The BCGs are, clearly, rather unusual entities, and the formation processes during the much higher-density regime of  $z \gtrsim 5$  are entirely likely to have been different from those at  $z \lesssim 2$  which gave rise to the main population of galaxies that we now see. A fully realistic model of a BCG-type protogalaxy during the epoch of globular cluster formation and galactic wind outflow, in all its undoubted complexity, is far beyond the scope of this paper (or indeed any current models). However, we can roughly quantify the effect on the specific frequency as follows: from Eqs. (4), (10), and (11), we obtain

$$S_N = 85.5 \times 10^6 \left( \frac{M}{L} \right)_V \epsilon \left( 1 + \frac{M_{gas}}{M_{stars}} \right) \quad (16)$$

where  $(M/L)_V$  is the mass-to-light ratio for the stellar material in an E galaxy; we adopt  $(M/L)_V = 8$  (Faber & Gallagher 1979; Binney & Tremaine 1987).  $M_{gas}$  is the amount of gas assumed to have been driven out by the galactic wind and unused for star formation. With the explicit assumption  $\epsilon \simeq const$ , Eq. (16) can be rewritten as

$$S_N = S_N^0 \left( 1 + \frac{M_{gas}}{M_{stars}} \right) \quad (17)$$

where  $S_N^0$  represents the fiducial specific frequency for a galaxy in which little or no gas is ejected and the star formation runs to completion ( $M_{gas} \ll M_{stars}$ ). Lacking a full physical theory, we must estimate  $S_N^0$  on observational grounds:

(a) The mean specific frequency for 14 large ellipticals in Virgo, Fornax, and the NGC 5846 group (from data in Harris & Harris 1997; see also Harris 1991; Kissler-Patig *et al.* 1997) is  $\langle S_N \rangle = 5.4 \pm 0.3$ , excluding the cD's M87 and NGC 1399. Since even the normal ellipticals have probably lost some of their original gas to early winds, this value should give an upper limit to  $S_N^0$ . An extreme *lower* limit can be set at  $S_N^0 \sim 2$ , which is the mean for the lowest specific frequencies found in a range of E and dE galaxies in sparse groups. A straight mean over *all* the non-BCG galaxies, weighted inversely as the observational uncertainty in  $S_N$ , gives  $\langle S_N \rangle = 3.3 \pm 0.2$ .

(b) The mean specific frequency for 13 dwarf ellipticals more luminous than  $M_V^T \simeq -15$  (Durrell *et al.* 1996) is  $\langle S_N \rangle = 4.2 \pm 0.5$ . These same dE's are small enough to have lost

typically  $\gtrsim 20\%$  of their initial gas in a wind, according to published models (e.g. Gibson 1997).<sup>7</sup> However, they may also have later destroyed a significant fraction of their original number of globular clusters by dynamical friction, since the GCS in a dwarf elliptical is quite centrally concentrated (see the discussion of Durrell *et al.*). These two effects have opposite and comparable influences on  $S_N$ , and it is not immediately clear which will be the more important over a Hubble time.

Taking the preceding arguments to bracket our estimate of  $S_N^0$ , we adopt  $S_N^0 = 3.5 \pm 1$ . (Similar ‘baseline’ values for  $S_N^0$  were reached by West *et al.* 1995 and BTM97, though for different reasons.) From Eq. (16), we find that the corresponding fiducial cluster formation efficiency is  $\epsilon \simeq 5.8 \times 10^{-9} M_\odot^{-1}$ , or one globular cluster per  $1.7 \times 10^8 M_\odot$  of gas. For a mean cluster mass  $\simeq 3 \times 10^5 M_\odot$  (from HP94; Harris 1996a; Meylan & Heggie 1997), the corresponding *specific mass* ratio as defined by HP94 is  $S_M = M_{GCS}/M_{stars} = 1.8 \times 10^{-3}$ . This result agrees extremely well with the observations from contemporary star-forming regions in the Milky Way and M31, in which the mass of gas seen to be forming clusters in giant molecular clouds is about  $2 \times 10^{-3}$  of the total GMC mass (HP94; McLaughlin 1997).

The value of  $S_N^0$  indicates that only 0.2% of the stellar mass in a typical E galaxy today is in the form of bound star clusters. To obtain a case like M87 with  $S_N \sim 14$ , we must then require  $(M_{gas}/M_{stars}) \simeq 3$ , i.e. that 75% of the original gas supply in the protogalaxy was ejected to rejoin the ICM. More generally, if  $M_{gas}$  equals the amount expelled by the wind, then the fraction  $f_M$  of the *initial protogalactic gas* that is lost is  $f_M = M_{gas}/(M_{gas} + M_{stars}) = 1 - (S_N^0/S_N)$ . This quantity, for our BCG sample, is shown in Fig. 16. For comparison, the expected dependence of  $f$  on  $\sigma$  derived from the scaling relations Eqs. (7-9) above is shown by the dashed line. A rough linear relation  $f_M \sim (\sigma_{cl}/1200 \text{ km s}^{-1})$  as shown in the graph matches equally well, given the observational scatter.

From this graph, we see again that to save the assumption  $\epsilon \sim \text{const}$ , we have to claim that quite a substantial fraction of the initial gas mass was expelled from the biggest systems. In terms of the total gas mass in the ICM, this is not at all an excessive requirement, since large Abell-type clusters typically contain  $\sim 10^{13} - 10^{14} M_\odot$  of diffuse gas, most of which is likely to be primordial material never processed through galaxies (e.g. David *et al.* 1991; Whitmore *et al.* 1993a). We recognize, however, that this requirement imposes very strong demands on the early SNII rate which will have to be put to the test

---

<sup>7</sup>Among dwarf E galaxies with globular cluster systems of their own, the lowest-luminosity dE’s have the highest specific frequencies (Durrell *et al.* 1996), the most extreme cases being the Fornax and Sagittarius dwarfs with  $S_N \sim 25$ . These tiny systems are likely to be ones which expelled most of their original gas in a single early burst (Dekel & Silk 1986).

in more advanced modelling.

Lastly, we explore the dependence of total GCS size on the *total* core mass in the surrounding cluster including the dark matter. For an isothermal potential well, the central density is given by  $\rho_c = 9\sigma^2/4\pi Gr_c^2$  where  $r_c$  is the *projected* core radius that we directly observe. The cluster core radii are known empirically (BTM97; Schaeffer *et al.* 1993) to scale approximately as  $r_c \simeq 104 \text{ kpc} (\sigma/500 \text{ km s}^{-1})^{0.6}$ . Thus we obtain

$$\rho_c \simeq 3.86 \times 10^{-3} M_\odot \text{ pc}^{-3} \left( \frac{\sigma_{cl}}{500 \text{ km s}^{-1}} \right)^{0.8}. \quad (18)$$

and the total mass contained within the core is

$$M_{core} \simeq \frac{4}{3}\pi r_c^3 \rho_c = 1.8 \times 10^{13} M_\odot \left( \frac{\sigma_{cl}}{500 \text{ km s}^{-1}} \right)^{2.6}. \quad (19)$$

$M_{core}$  is of course dominated by the dark matter, with smaller contributions from the visible galaxy and the X-ray gas. Since the core radii are typically of order  $\sim 100$  kpc,  $\rho_c$  defined in this way comfortably encloses the bulk of the central BCG and provides a reasonable representation of the overall mass density there. In Fig. 17 we show the ratio  $M_{core}/N_{GC}$ , the *total mass per unit globular cluster*, plotted against velocity dispersion. The graph indicates that the globular cluster formation efficiency *in an absolute sense* (number per unit total mass,  $M_{core} = M_{gas} + M_{stars} + M_{dark}$ ) is *lower* in the more massive BCGs. This result is consistent with our suggestion that the galactic wind may have been earlier and more effective in the more massive environments, possibly interrupting even the GCS formation before it could run to completion.

This conclusion about the absolute efficiency of globular cluster formation is not the same as in BTM97. This apparent disagreement is due primarily to different definitions of terms. They defined an efficiency ratio using a *projected* core mass  $M_c$  over a cylindrical volume, derived from the surface density  $\Sigma_c$  rather than  $\rho_c$ . In addition, they calculated  $M_c$  for a fixed radius of 40 kpc in all clusters. We believe it is more appropriate to use a total core mass calculated from a true three-dimensional mass density, in order to compare with the total globular cluster population in the entire BCG. For the sake of more direct comparison, we show in the lower panel of Fig. 17 the ratio  $M^{100}/N_{GC}$ , where  $M^{100}$  is the total mass within a fixed (spherical, not cylindrical) volume of radius of 100 kpc, which roughly represents the total optical extent of these galaxies. In the sense defined by  $M^{100}$ , the absolute efficiency increases with  $\sigma_{cl}$ , though the trend is less obvious than in the upper panel. It is not clear to us which of the two representations is preferable; in either graph, a typical mass ratio is about  $3 \times 10^9 M_\odot$  per globular cluster. Comparing this value with the mean  $\epsilon^{-1} \sim 2 \times 10^8 M_\odot$  (gas mass per globular cluster) derived above, we see that the dark matter makes up  $\gtrsim 90\%$  of the total mass even within the cluster core.

The scenario we have outlined here explores the implications of a single important assumption: that the conversion rate  $\epsilon$  of protogalactic gas into globular clusters was statistically uniform in different environments. Pursuing this assumption leads to the hypothesis that BCGs ejected a much higher fraction of their initial gas mass than did more normal E galaxies. We recognize that this discussion is highly speculative, and is supported only in an indirect sense by the GCS scaling relations which are just now beginning to emerge from the data.

The obvious alternative to this admittedly risky conclusion is simply to assume that  $\epsilon$  is strongly dependent on environment, varying by up to an order of magnitude in different E galaxies. As yet, there are no definitive arguments either to rule out such a view or to clearly support it. The galactic wind hypothesis is offered as an alternate approach, which does have the advantage of connecting to a known major event in the early history of a large E galaxy.

## 6. SUMMARY

We have conducted a photometric study of the inner-halo globular cluster system in the Virgo giant M87, and have used the characteristics of its GCS as the starting point for a discussion of the formation of central cluster galaxies like it. A summary of our principal findings is as follows:

- (1) The luminosity distribution of the globular clusters in M87 (in its form either as the GCLF or the LDF) is virtually independent of location in the halo for *any* projected radius  $r \gtrsim 1$  kpc. We suggest that the main effects of dynamical evolution (tidal shocking and evaporation) may be limited to clusters less massive than  $M_{cl} \lesssim 10^5 M_\odot$ , below the faint limits of the present data. Alternatively, cluster evolution has proceeded in such a way as to preserve the overall shape of the GCLF as a function of time, as the recent model simulations are beginning to show. Dynamical friction may have removed the very most massive clusters ( $M \gtrsim 2 \times 10^6 M_\odot$ ) in the innermost few kiloparsecs.
- (2) Within  $\sim 4$  kpc of the galaxy center, the mean metallicity of the GCS is uniform with radius at the metal-rich level of  $[\text{Fe}/\text{H}] \simeq -0.3$ . At larger radii, the mean cluster metallicity declines as  $(Z/Z_\odot) \sim r^{-0.9}$ . We find that cluster metallicity is largely uncorrelated with cluster luminosity.
- (3) M87 holds the paradigmatic high-specific-frequency globular cluster system. We examine carefully the hypothesis that its many thousands of “extra” globular clusters are due to an intergalactic (IGC) population in the Virgo potential well, and reject it. The

dominant quantitative problem with the IGC model is that it requires the intracluster globulars to have a highly unrealistic spatial distribution, inconsistent with the assumptions of the model. We conclude that the vast majority of the globular clusters within M87 belong to it, and were formed with it *in situ*.

(4) Adding the recent results of Blakeslee (1997) and Blakeslee *et al.* (1997) to other data from the literature, we reinforce the result that GCSs in “brightest cluster galaxies” like M87 become continuously more populous (higher specific frequency) with parent galaxy size, and with the total mass of the surrounding galaxy cluster. However, the absolute *efficiency* of GCS formation (measured as the number of globular clusters per unit mass in the cluster core) *decreases* with increasing core mass. We use the available observations for 30 BCGs to construct empirical scaling relations describing the globular cluster population and specific frequency as a function of cluster mass (measured by the velocity dispersion  $\sigma_{cl}$  of the galaxies).

(5) We suggest that globular cluster specific frequency in BCGs may have been strongly influenced by the early galactic wind driven by the first round of Type II supernovae throughout the protogalaxy. In particular, we speculate that BCGs differed from normal ellipticals by generating a higher early star formation rate. The considerably stronger resulting wind interrupted subsequent star formation, drove out a large fraction of the initial gas mass, and left behind a galaxy with a higher than average ratio of globular clusters to field stars. If this hypothesis proves to be invalid, the most obvious alternative is to require that the GCS formation efficiency per unit gas mass ( $\epsilon$ ) was higher in BCGs than in normal ellipticals, and in general becomes progressively higher in larger-density environments.

This research was supported through grants to W.E.H. and G.L.H.H. from the Natural Sciences and Engineering Research Council of Canada. Additional support was provided to D.E.M. by NASA through grant number HF-1097.01-97A awarded by the Space Telescope Science Institute, which is operated by the Association of Universities for Research in Astronomy, Inc., for NASA under contract NAS5-26555.

## REFERENCES

- Ajhar, E. A., Blakeslee, J. P., & Tonry, J. L. 1994, *AJ*, 108, 2087
- Arimoto, N., & Yoshii, Y. 1987, *A&A*, 173, 23
- Armandroff, T. E. 1989, *AJ*, 97, 375
- Arnaboldi, M., *et al.* 1996, *ApJ*, 472, 145
- Arnaud, M., Rothenflug, R., Boulade, O., Vigroux, L., & Vangioni-Flam, E. 1992, *A&A*, 254, 49
- Ashman, K. M., & Zepf, S. E. 1992, *ApJ*, 384, 50
- Bender, R., Ziegler, B., & Bruzual, G. 1996, *ApJ*, 463, L51
- Binggeli, B., Tammann, G. A., & Sandage, A. 1987, *AJ*, 94, 251
- Binney, J., & Tremaine, S. 1987, *Galactic Dynamics* (Princeton University Press, Princeton)
- Blakeslee, J. P. 1997, *ApJ*, 481, L59 (B97)
- Blakeslee, J. P., Tonry, J. L., & Metzger, M. R. 1997, *AJ*, 114, 482 (BTM97)
- Bridges, T. E., Hanes, D., & Harris, W. E. 1991, *AJ*, 101, 469
- Bridges, T., Carter, D., Harris, W. E., & Pritchett, C. J. 1996, *MNRAS*, 281, 1290
- Burstein, D., & Heiles, C. 1984, *ApJS*, 54, 33
- Capriotti, E. R., & Hawley, S. L. 1996, *ApJ*, 464, 765
- Capuzzo-Dolcetta, R. 1993, *ApJ*, 415, 616
- Capuzzo-Dolcetta, R., & Tisseri, A. 1997, *MNRAS* (in press)
- Capuzzo-Dolcetta, R., & Vignola, L. 1997, *A&A* (in press)
- Carretta, E., & Gratton, R. G. 1997, *A&AS*, 121, 95
- Carter, D., & Dixon, K. L. 1978, *AJ*, 83, 6
- Christian, C. A., Adams, M., Barnes, J. V., Butcher, H., Hayes, D. S., Mould, J. R., & Siegel, M. 1985, *PASP*, 97, 363
- Ciardullo, R., Jacoby, G. H., Feldmeier, J. J., & Bartlett, R. E. 1998, *ApJ*, 492, 62

- Cohen, J. G., & Ryzhov, A. 1997, *ApJ*, 486, 230
- Côté, P., Marzke, R. O., & West, M. J. 1998, *ApJ*, in press
- Couture, J., Harris, W. E., & Allwright, J. W. B. 1990, *ApJS*, 73, 671
- David, L. P., Forman, W., & Jones, C. 1990, *ApJ*, 356, 32
- David, L. P., Forman, W., & Jones, C. 1991, *ApJ*, 380, 39
- Davis, D. S., & White, R. E. III 1996, *ApJ*, 470, L35
- Davis, L. 1990, private communication
- Dekel, A., & Silk, J. 1986, *ApJ*, 303, 39
- de Vaucouleurs, G. 1975, in *Galaxies and the Universe*, edited by A. Sandage, M. Sandage, and J. Kristian (Univ.Chicago Press, Chicago), p. 557
- de Vaucouleurs, G., & Nieto, J.-L. 1978, *ApJ*, 220, 449
- Di Fazio, A. 1986, *A&A*, 159, 49
- Durrell, P. R., Harris, W. E., Geisler, D., & Pudritz, R. E. 1996, *AJ*, 112, 972
- Ellis, R. S. *et al.* 1997, *ApJ*, 483, 582
- Elmegreen, B. G., & Efremov, Y. N. 1997, *ApJ*, 480, 235
- Elmegreen, B. G., & Falgarone, E. 1996, *ApJ*, 471, 816
- Elson, R. A., & Santiago, B. X. 1996a, *MNRAS*, 278, 617
- Elson, R. A., & Santiago, B. X. 1996b, *MNRAS*, 280, 971
- Faber, S. M., & Gallagher, J. 1979, *ARA&A*, 17, 135
- Fabian, A. C., Nulsen, P. E. J., & Canizares, C. R. 1984, *Nature*, 310, 733
- Fabian, A. C., Crawford, C., Edge, A., & Mushotzky, R. 1994, *MNRAS*, 267, 779
- Fadda, D., Girardi, M., Giuricin, G., Mardirossian, F., & Mezzetti, M. 1996, *ApJ*, 473, 670
- Ferguson, H., Tanvir, N., & von Hippel, T. 1996, *BAAS*, 189, 8006
- Fleming, D. E. B., Harris, W. E., Pritchett, C. J., & Hanes, D. A. 1995, *AJ*, 109, 1044

- Forbes, D. A. 1996a, AJ, 112, 954
- Forbes, D. A. 1996b, AJ, 112, 1409
- Forbes, D. A., Brodie, J. P., & Huchra, J. 1997, AJ, 113, 887
- Forbes, D. A., Franx, M., Illingworth, G. D., & Carollo, C. M. 1996, ApJ, 467, 126
- Geisler, D., Lee, M. G., & Kim, E. 1996, AJ, 111, 1529
- Geller, M. J., & Huchra, J. P. 1983, ApJS, 52, 61
- Giavalisco, M., Steidel, C. C., & Macchetto, F. D. 1996, ApJ, 470, 189
- Gibson, B. K. 1994, JRASC, 88, 383
- Gibson, B. K. 1996, ApJ, 468, 167
- Gibson, B. K. 1997, preprint (astroph-9705104)
- Girardi, M., Biviano, A., Giuricin, G., Mardirossian, F., & Mezzetti, M. 1993, ApJ, 404, 38
- Gnedin, O. Y., & Ostriker, J. P. 1997, ApJ, 474, 223
- Grillmair, C. *et al.* 1994a, AJ, 108, 102
- Grillmair, C. J. *et al.* 1994b, ApJ, 422, L9
- Hanes, D. A. 1977, MNRAS, 180, 309
- Hanes, D. A., & Harris, W. E. 1986, ApJ, 309, 564
- Harris, G. L. H., Geisler, D., Harris, H. C., & Hesser, J. E. 1992, AJ, 104, 613
- Harris, H. C., & Harris, W. E. 1998, in *Astrophysical Quantities*, 4th ed., edited by A.N.Cox (in press)
- Harris, W. E. 1981, ApJ, 251, 497
- Harris, W. E. 1986, AJ, 91, 822
- Harris, W. E. 1991, ARA&A, 29, 543
- Harris, W. E. 1995, in *Stellar Populations*, IAU Symposium No. 164, edited by P.C.van der Kruit and G.Gilmore (Kluwer, Dordrecht), p.85
- Harris, W. E. 1996a, AJ, 112, 1487

- Harris, W. E. 1996b, in *The Extragalactic Distance Scale*, edited by M. Livio, M. Donahue, and N. Panagia (Space Telescope Science Institute, Baltimore)
- Harris, W. E., Allwright, J. W. B., Pritchet, C. J., & van den Bergh, S. 1991, *ApJS*, 76, 115
- Harris, W. E., & Petrie, P. L. 1978, *ApJ*, 223, 88
- Harris, W. E., Pritchet, C. J., & McClure, R. D. 1995, *ApJ*, 441, 120
- Harris, W. E., & Pudritz, R. E. 1994, *ApJ*, 429, 177 (HP94)
- Harris, W. E., & Racine, R. 1979, *ARA&A*, 17, 241
- Harris, W. E., & Smith, M. G. 1976, *ApJ*, 207, 1036
- Harris, W. E., & van den Bergh, S. 1981, *AJ*, 86, 1627
- Hesser, J. E., Harris, H. C., van den Bergh, S., & Harris, G. L. H. 1984, *ApJ*, 276, 491
- Holtzman, J. A. *et al.* 1992, *AJ*, 103, 691
- Holtzman, J. A. *et al.* 1996, *AJ*, 112, 416
- Jacoby, G. H. *et al.* 1992, *PASP*, 104, 599
- Kaisler, D., Harris, W. E., Crabtree, D. R., & Richer, H. B. 1996, *AJ*, 111, 2224
- Kavelaars, J. J., & Hanes, D. A. 1997, *MNRAS*, 285, L31
- Killeen, N. E. B., & Bicknell, G. V. 1988, *ApJ*, 325, 165
- Kissler-Patig, M., Kohle, L., Hilker, M., Richtler, T., Infante, L., & Quintana, H. 1997, *A&A*, 319, 470
- Kissler-Patig, M., Richtler, T., & Hilker, M. 1996, *A&A*, 308, 704
- Kissler-Patig, M. 1998, in *Galactic Halos*, ASP Conf. Ser., edited by D. Zaritsky (ASP, San Francisco), in press
- Kumai, Y., Basu, B., & Fujimoto, M. 1993a, *ApJ*, 404, 144
- Kumai, Y., Hashi, Y., & Fujimoto, M. 1993b, *ApJ*, 416, 576
- Larson, R. B. 1974, *MNRAS*, 169, 229
- Larson, R. B. 1990a, *PASP*, 653, 704

- Larson, R. B. 1990b, in *Physical Processes in Fragmentation and Star Formation*, edited by R. Capuzzo-Dolcetta, C. Chiosi, and A. DiFazio (Kluwer, Dordrecht), p.389
- Larson, R. B. 1993, in *The Globular Cluster – Galaxy Connection*, ASP Conf. Ser. 48, edited by G. H. Smith and J. P. Brodie (ASP, San Francisco), p. 675
- Lauer, T. R., & Kormendy, J. 1986, *ApJ*, 303, L1
- Lee, M. G., & Geisler, D. 1993, *AJ*, 106, 493
- Loewenstein, M., & Mushotzky, R. F. 1996, *ApJ*, 466, 695
- López-Cruz, O., Yee, H. K. C., Brown, J. P., Jones, C., & Forman, W. 1997, *ApJ*, 475, L97
- Maoz, E. 1990, *ApJ*, 359, 257
- Mathews, W. G., & Baker, J. C. 1971, *ApJ*, 170, 241
- Matteucci, F., & Gibson, B. K. 1995, *A&A*, 304, 11
- McClure, R. D. *et al.* 1989, *PASP*, 101, 1156
- McLaughlin, D. E. 1994, *PASP*, 106, 47
- McLaughlin, D. E. 1995, *AJ*, 109, 2034
- McLaughlin, D. E. 1997, PhD thesis, McMaster University.
- McLaughlin, D. E., Harris, W. E., & Hanes, D. A. 1993, *ApJ*, 409, L45
- McLaughlin, D.E., Harris, W.E., & Hanes, D.A. 1994, *ApJ*, 422, 486
- McLaughlin, D. E., & Pudritz, R. E. 1996, *ApJ*, 457, 578
- Mendez, R. H. *et al.*, *ApJ*, 491, L23
- Merritt, D. 1984, *ApJ*, 276, 26
- Meylan, G., & Heggie, D. C. 1997, *A&AR*, 8, 1
- Miller, B. W., Whitmore, B. C., Schweizer, F., & Fall, S. M. 1997, *AJ*, 114, 2381
- Minniti, D., Kissler-Patig, M., Goudfrooij, P., & Meylan, G. 1998, *AJ*, 115, in press
- Morbey, C. L., & McClure, R. D. 1985, *PASP*, 97, 110
- Murali, C., & Weinberg, M. D. 1997, *MNRAS*, 288, 749

- Mushotzky, R. F., & Loewenstein, M. 1997, *ApJ*, 481, L63
- Muzzio, J. C. 1987, *PASP*, 99, 245
- Okazaki, T., & Tosa, M. 1995, *MNRAS*, 274, 48
- Ostriker, J. P., & Gnedin, O. Y. 1997, *ApJ*, 487, 667
- Renzini, A., Ciotti, L., D’Ercole, A., & Pellegrini, S. 1993, *ApJ*, 419, 52
- Schaeffer, R., Maurogordato, S., Cappi, A., & Bernardeau, F. 1993, *MNRAS*, 263, L21
- Schild, R. E. 1983, *PASP*, 95, 1021
- Schombert, J. M. 1988, *ApJ*, 328, 475
- Schweizer, F. 1987, in *Nearly Normal Galaxies*, edited by S.M.Faber (Springer-Verlag, New York), p.18
- Schweizer, F. 1997, in *The Nature of Elliptical Galaxies, Proceedings of the Second Stromlo Symposium*, edited by M.Arnaboldi, G.S.Da Costa, and P.Saha (in press)
- Schweizer, F., Miller, B. W., Whitmore, B. C., & Fall, S. M. 1996, *AJ*, 112, 1839
- Searle, L., & Zinn, R. 1978, *ApJ*, 225, 357
- Secker, J. 1992, *AJ*, 104, 1472
- Sembach, K. R., & Tonry, J. L. 1996, *AJ*, 112, 797
- Steidel, C. C., Giavalisco, M., Pettini, M., Dickinson, M., & Adelberger, K. L. 1996, *ApJ*, 462, L17
- Stetson, P. B. 1992, in *Astronomical Data Analysis Software and Systems I*, ASP Conf. Ser. 8, edited by G. H. Jacoby (ASP, San Francisco), p. 289
- Theuns, T., & Warren, S. J. 1997, *MNRAS*, 284, L11
- Thuan, T. X., & Kormendy, J. 1977, *PASP*, 89, 466
- Tremaine, S. D., Ostriker, J. P., & Spitzer, L. 1975, *ApJ*, 196, 407
- Turner, E. L. 1991, *AJ*, 101, 5
- van den Bergh, S. 1977, *Vistas in Astronomy*, 21, 71

- van den Bergh, S. 1984, *PASP*, 96, 329
- Vesperini, E. 1997, *MNRAS*, 287, 915
- West, M. J. 1993, *MNRAS*, 265, 755
- West, M. J., Côté, P., Jones, C., Forman, W., & Marzke, R. O. 1995, *ApJ*, 453, L77
- White, R. E. 1987, *MNRAS*, 227, 185
- Whitmore, B. C. 1996, in *The Extragalactic Distance Scale*, edited by M. Livio, M. Donahue, and N. Panagia (Space Telescope Science Institute, Baltimore)
- Whitmore, B. C., Gilmore, D. M., & Jones, C. 1993a, *ApJ*, 407, 489
- Whitmore, B. C., & Schweizer, F. 1995, *AJ*, 109, 960
- Whitmore, B. C., Schweizer, F., Leitherer, C., Borne, K., & Robert, C. 1993b, *AJ*, 106, 1354
- Whitmore, B. C., Sparks, W. B., Lucas, R. A., Macchetto, F. D., & Biretta, J. A. 1995, *ApJ*, 454, L73
- Zepf, S., & Ashman, K. M. 1993, *MNRAS*, 264, 611
- Zepf, S. E., Ashman, K., & Geisler, D. 1995, *ApJ*, 443, 570
- Zinn, R. 1985, *ApJ*, 293, 424

### Figure Captions

Fig. 1.—  $R$ -band image of the central field in M87. This frame is a median of 26 individual 500-sec exposures in  $R$  taken with the CFHT and HRCam at prime focus (see Sec. 2.2 of the text). North is approximately at the upper right corner, East at lower right; see Fig. 2 for a finder chart with an exact orientation map. The large black dot along the left edge of the field is the hole enclosing the bright guide star for the tip-tilt correction of the camera. The smooth isophotal contours of the galaxy have been subtracted through an ellipse-fitting model (see Sec. 3).

Fig. 2.— Distribution of starlike objects in the M87 central field that are brighter than the GCLF turnover ( $R \lesssim 23.2$ ). Larger symbols correspond to brighter objects; compare with the direct image of Fig. 1. Fiducial directions are marked on the borders, with the galaxy center at (0,0). The concentric circles have successive radii of  $9''.2$ ,  $19''.7$ ,  $39''.3$ , and  $59''.0$ , defining the four radial zones used in the GCLF analysis. Note the small sector directly above the galaxy center with no measured objects: this sector contains the nuclear jet and was excluded from any analysis.

Fig. 3.— Completeness of image detection in each annular zone, as a function of  $R$  magnitude. These curves are the empirical results of artificial-star tests as described in Sec. 2.2. The five zones are defined in Table 4: Ring 1 is the innermost zone and B denotes the remote background field.

Fig. 4.— Internal precision of the  $R$ -band photometry, as derived from the artificial-star tests. Here  $\sigma(R)$  is rms scatter in the measured magnitudes of the recovered stars. The data are plotted (unsmoothed) in 0.5-mag steps, with the five zones labelled as in the previous figure.

Fig. 5.— GCLFs for the four zones defined in Table 4. In each bin, the number of globular clusters per 0.4-mag bin, fully corrected for detection incompleteness and background subtraction, is plotted against  $R$  magnitude.

Fig. 6.— (a) *Upper panel*: The GCLF for the three zones 2-4 combined. A Gaussian curve with peak at  $R_0 = 23.2$  and dispersion  $\sigma = 1.4$  mag as derived from Whitmore *et al.* (1995) and the present data is superimposed on the datapoints. (b) *Lower panel*: The GCLF for the innermost ring. Two Gaussian curves with the same peak but different dispersions are compared: the narrower curve with  $\sigma = 0.75$  provides the formal best fit, but the wider one which matches the outer zones cannot be strongly ruled out.

Fig. 7.— Luminosity distribution function (LDF) for the M87 globular clusters in three

regions of the halo. Here  $dN/dL$  represents the number of clusters per unit luminosity, plotted against cluster luminosity in Solar units ( $L/L_\odot$ ); the three sets of points have been shifted vertically by arbitrary amounts for clarity. Solid circles are the data from ring 1 (projected radii 0.7 – 1.4 kpc); open circles are from rings 2 – 4 (1.4 – 10.3 kpc); and solid triangles are outer-halo GCS data ( $r > 10$  kpc) from McLaughlin *et al.* (1994). Note the similarity of the LDF slope in all three regimes over most of the luminosity range, coupled with a progressive disappearance of the most luminous clusters ( $\log(L/L_\odot) \gtrsim 6.2$ ) going inward toward smaller radii.

Fig. 8.— Color-magnitude distribution for the measured objects in the M87 central field;  $R$  is plotted against  $(V - R)$ ,  $(R - I)$ , and  $(V - I)$ . In the last panel, the two peaks in the bimodal color distribution noted by Elson & Santiago (1996b) and Whitmore *et al.* (1995) are indicated by dashed lines. Most of our objects belong to the redder, more metal-rich group since they are in the inner halo; see text.

Fig. 9.— Mean  $(V - I)$  colors of the globular clusters as a function of magnitude. The dashed arrow at  $R \sim 21.5$  marks the magnitude near which Elson & Santiago (1996b) found an extra “clump” of clusters in the blue part of the bimodal color distribution.

Fig. 10.— Metallicity gradient for the globular cluster system in M87, combining the inner-halo data from this study (solid symbols) and the outer-halo data from Lee & Geisler (1993) (open symbols). Note that within one core radius  $r_c \simeq 1'$ , there is no change in the mean cluster metallicity; at larger radii, there is a steady decrease in mean metallicity out to the limits of the observations, scaling roughly as  $Z \sim r^{-0.9}$ .

Fig. 11.— Total number of globular clusters plotted against galaxy luminosity, for elliptical galaxies. *Open circles* indicate giant ellipticals which are the centrally dominant members of their clusters (BCGs). *Solid dots* indicate all other E-type galaxies, including dwarfs. The solid line is a direct proportionality  $N_{GC} \sim L_{gal}$  for a specific frequency  $S_N^0 = 3.5$ . See Sec. 5.4 of the text.

Fig. 12.— Specific frequency  $S_N$  plotted against the X-ray temperature of the ICM gas. Open symbols are BCGs taken from Table 6. Solid symbols are BCGs taken from the Blakeslee *et al.* (1997) sample, where we have converted their metric  $S_N^{40}$  to the global specific frequency via  $S_N = 1.3S_N^{40}$  (see Sec. 5.4).

Fig. 13.— (a) *Upper panel:* BCG specific frequency plotted against the velocity dispersion  $\sigma_{cl}$  of the galaxies in the cluster. Solid symbols are the BTM97 sample, and open symbols are taken from Table 6 as above. The solid line shows the scaling relation from Eq. (6). (b) *Lower panel:* Total cluster population  $N_{GC} \sim L \cdot S_N$  plotted against  $\sigma_{cl}$ . Symbols are as

above. The solid line shows the scaling relation from Eq. (17).

Fig. 14.— Radial profile of the M87 halo light, deconvolved into ‘body’ and ‘envelope’ components as described in Sec. 5.4 of the text. Solid dots represent the  $B$ -magnitude surface intensity profile of Carter & Dixon (1978); open symbols represent the  $B$  measurements of de Vaucouleurs & Nieto (1978). The extended envelope component, defined to fit the Carter-Dixon data, is assumed to be intracluster light in the overall potential well of the Virgo cluster; see text.

Fig. 15.— (a) *Upper panel*: Specific frequency profiles for the globular cluster systems of M87 (solid symbols) and M49 (open symbols), as described in Sec. 5.4 of the text. A model for the M87 GCS is assumed here in which the main body of the galaxy has a normal M49-like specific frequency, while the intergalactic globular clusters from the extended envelope raise the total specific frequency up to the observed value  $S_N^{tot}$ . Both sets of data are taken from Fig. 21 of McLaughlin *et al.* (1994), and have been properly scaled to reflect a Virgo distance modulus of  $(m - M)_V = 31.0$  and the same GCLF turnover and dispersion as adopted in Sec. 3. (b) *Lower panel*: Deduced specific frequency profile for the IGC (envelope) component, obtained from the difference between the top and bottom curves in panel (a). The assumed IGCs are required to have an extremely high overall  $S_N$ , and to be concentrated toward the galaxy nucleus.

Fig. 16.— Mass fraction  $f_M = 1 - (S_N^0/S_N)$  plotted against  $\sigma_{cl}$ . According to the galactic wind hypothesis discussed in Sec. 5.5,  $f_M$  is the fraction of the initial protogalactic gas lost to the ICM,  $f_M = M_{gas}/(M_{gas} + M_{stars})$ . The *dashed line* indicates the predicted dependence of  $f$  on  $\sigma$  from the scaling relations in Eqs. (7-9), while the *solid line* shows the more approximate linear relation defined in the text.

Fig. 17.— (a) *Upper panel*: Ratio of total core mass in the cluster of galaxies to globular cluster population, plotted against velocity dispersion. See Sec. 5.5. (b) *Lower panel*: Ratio of “metric” core mass (within 100 kpc radius) to  $N_{GC}$ , plotted against velocity dispersion.